# Section 1

# Atmospheric data assimilation schemes, analysis and initialization, data impact studies, observing system experiments

# Data assimilation experiments of Myanmar cyclone Nargis based on NHM-LETKF

Le Duc[12], Tohru Koruda[12], Kazuo Saito[21], and Tadashi Fujita[3]

[1]Japan Agency for Marine-Earth Science and Technology, Yokohama, Japan; leduc@jamstec.go.jp

[2]Meteorological Research Institute, Tsukuba, Japan

[3]Japan Meteorological Agency, Tokyo, Japan

Nargis was a severe storm which formed in Bay of Bengal in April 2008 and made landfall in the Irrawaddy delta, resulting in massive damage and loss of life in Myanmar. After forming, Nargis followed the northwest direction until April 30th 2008 and turned to the east direction, intensified rapidly and made landfall with the estimated intensity of at least 165 km/h. All global forecasts missed this deflecting motion and rapid intensification. In this study, a data assimilation experiment based on the Local Ensemble Transform Kalman Filter (LETKF) and NHM model was performed to investigate this problem.

The NHM-LETKF system originally developed in JMA was adopted and modified in this study. The JMA nonhydrostatic model NHM (Saito et al., 2007) was used as the driving model in the system. The assimilation part followed the 4D-LETKF scheme as described by Hunt et al. (2007). This LETKF program supports adaptive inflation, adaptive vertical and horizontal localisation, and outer loop as options. Localisation is specified by two parameters: vertical and horizontal localisation scales, which when multiplied by $2\sqrt{10/3}$ yield the radii of vertical and horizontal scales. R-localisation was also implemented in the LETKF program. The control variable are u, v, t, qv, and ps. To apply the system to Nargis case, we introduced the Mercator projection into the system in addition to the default Lambert projection.

A domain with the resolution of 20km covering Bay of Bengal was chosen for the experiments. It has 201x161 grid points and 40 vertical levels. The domain and observations were used in the experiments are illustrated in Fig. 1. Forecasts from JMA's global deterministic model of the resolution of $0.5^0$ were used as the boundary conditions. The boundary perturbations were interpolated from JMA's 1-week ensemble prediction system. The initial seeds for all members were also given by initial perturbations this system. SST perturbations were introduced by using SST analyses from 7 centers: FNMOC, JMA, JPL, NCDC, NCEP, REMSS, and UKMO.

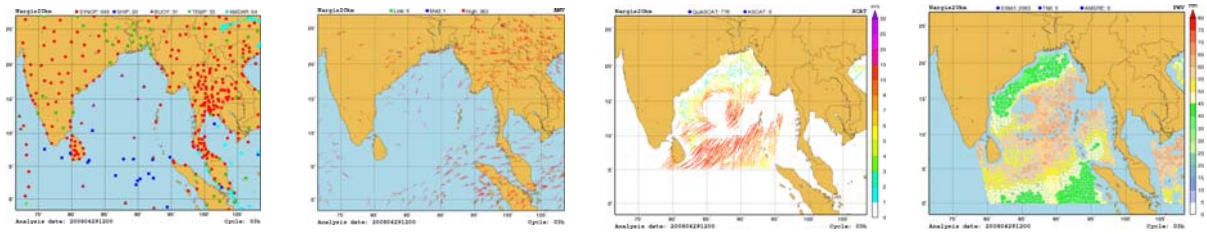

**Fig. 1.** Used observations at 18Z-20080429: conventional data, AMVs, sea winds, and retrieved precipitation water.

For all experiments here, we did not apply the outer loop or adaptive options. The configuration parameters were chosen as following: 50 ensemble members, the assimilation cycle of 3 hours, the horizontal localization scale of 5 (about 400 km radius). With two free remaining parameters: the multiplicative inflation factor (MIF) and the vertical localization scale (VLS), we performed sensitivity tests to find the appropriate values in Nargis case. In each experiment, the system was run from 12Z-28/04/2008 to 12Z-30/04/2004. Then the resulting analysis was used as the initial condition for 60-hour NHM forecast. To see the impact from NHM-LETKF, the

forecast downscaling from JMA global model was also carried out.

First of all, the system was checked with MIF of 1.21 (10%) and VLS of 12. Fig. 2 shows the performance of the system with these parameters. This figure says that the system worked properly when analysis root mean square errors (RMSE) and spreads were less than those of forecasts, resulting from assimilation. However, it also points out that the system is under-dispersive with a large gap between RMSEs and spreads.

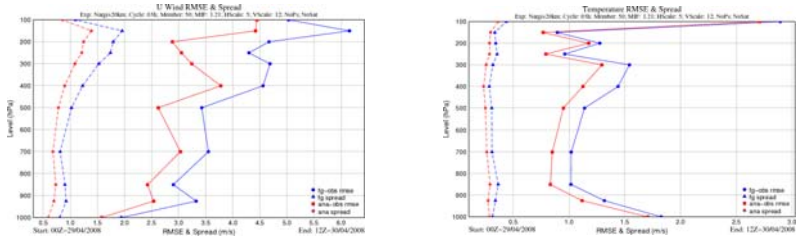

**Fig. 2.** Averaged RMSEs and spreads of forecasts and analyses at radiosonde stations with MIF of 10% and VLS of 12.

This under-dispersive property can be attributed to the sampling errors due to a limited number of ensemble member and the model errors, which was parameterized insufficient in the system. To alleviate this problem, MIFs should be increased. The impact of MIF increasing is illustrated in Fig. 3. It is clearly that the spreads increase while RMSEs slightly decrease with increasing MIF. In term of both Nargis track and intensity forecasts, MIF of 1.96 (40%) yields the best result.

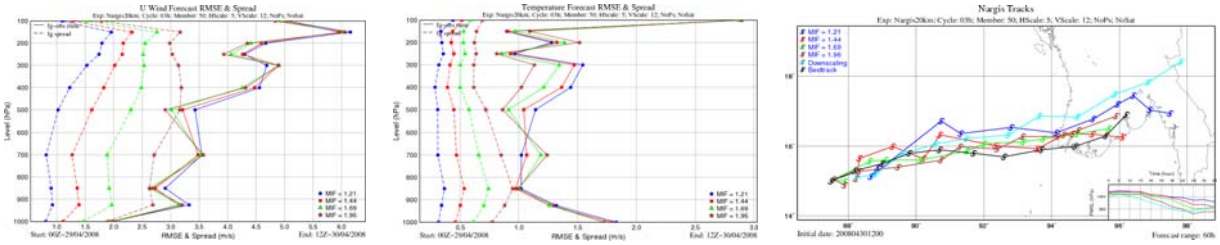

**Fig. 3.** Averaged RMSEs and spreads of u-wind (left) and temperature (center) forecasts at radiosonde stations, and Nargis track and intensity forecasts with different MIFs.

This under-dispersive property can also be cured by decreasing VLS. The sensitivity test of VLS was performed the same as the previous experiment with MIF (Fig. 4). As expected, spreads increased with decreasing VLS, however the impact on RMSEs is neutral. The interesting thing is that VLS increasing gives the better forecasted track and intensity, suggesting that in case of tropical cyclone, vertical localization scales should be large in LETKF.

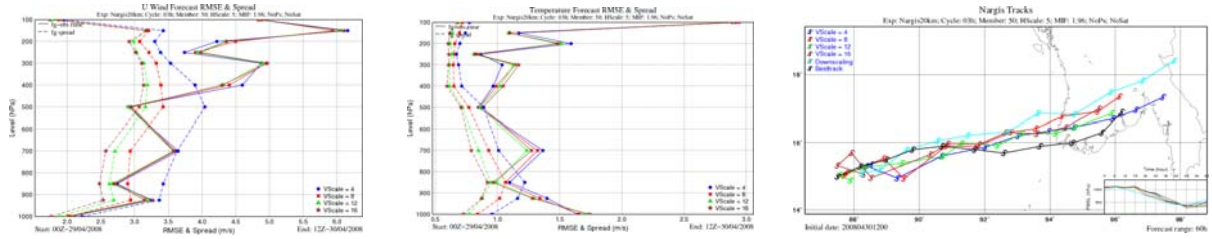

**Fig. 4.** Averaged RMSEs and spreads of u-wind (left) and temperature (center) forecasts at radiosonde stations, and Nargis track and intensity forecasts with different VLSs.

**Reference**


Hunt, B. R., E. J. Kostelich and I. Szunyogh, 2007: Efficient Data Assimilation for Spatiotemporal Chaos: A Local Ensemble Transform Kalman Filter. *Physica D*, **230**, 112-126.

Saito, K., Ishida J., Aranami K., Hara T., Segawa T., Narita M., and Honda Y., 2007: Nonhydrostatic atmospheric models and operational development at JMA. *J. Meteor. Soc. Japan.*, **85B**, 271–304.

# Radar reflectivity assimilation in JMA's operational meso-analysis system

Yasutaka Ikuta[1]

*Numerical Prediction Division, Japan Meteorological Agency*

The Japan Meteorological Agency (JMA) operates a meso-scale model (MSM) with a meso-analysis (MA) system to support the provision of additional information on disaster prevention. The MSM produces very short-range weather forecasts, and MA provides high-quality initial atmospheric conditions for it. In order to improve precipitation forecasting with the MSM, MA must be made to describe water vapor distribution in the initial condition more accurately. To this end, JMA started using radar reflectivity data in the operational MA system on June 9, 2011.

To assimilate radar reflectivity data in MA, an indirect assimilation technique called 1D+4DVAR (Ikuta and Honda 2011) is employed. In this method, radar reflectivity data are used to determine relative humidity (RH), and the RH values retrieved are assimilated as conventional observation data using 4DVAR. In this system, only RH retrievals below the melting layer are used because it is known that reflectivity is inappropriately simulated in the ice phase with the operational MSM hydrometeor forecast, and this causes large biases in RH data. In addition, data from around the 2,000 m level are not used because they are adopted to create radar/raingauge-analyzed precipitation data, which are assimilated in MA in another form (surface rainfall).

For operation, reflectivity data from JMA's C-band radar network (20 sites) are used. As shown in Figure 1, the retrieved RH data cover most of the Japanese archipelago.

The positive impact of the 1D+4DVAR approach using radar reflectivity is expected to improve the water vapor profile of initial conditions and to reduce displacement errors in the precipitation system (Ikuta and Honda 2011), and this was supported by the results of an eight-day pre-operational test of the method started on July 19, 2009. Figure 2 illustrates the reduction of displacement errors. The control and test experiments produced prediction results with and without assimilation of radar reflectivity data. The control showed a strong rain band off the coast of Kyushu, while the observation showed the band located along the coast. This displacement error was reduced in the test.

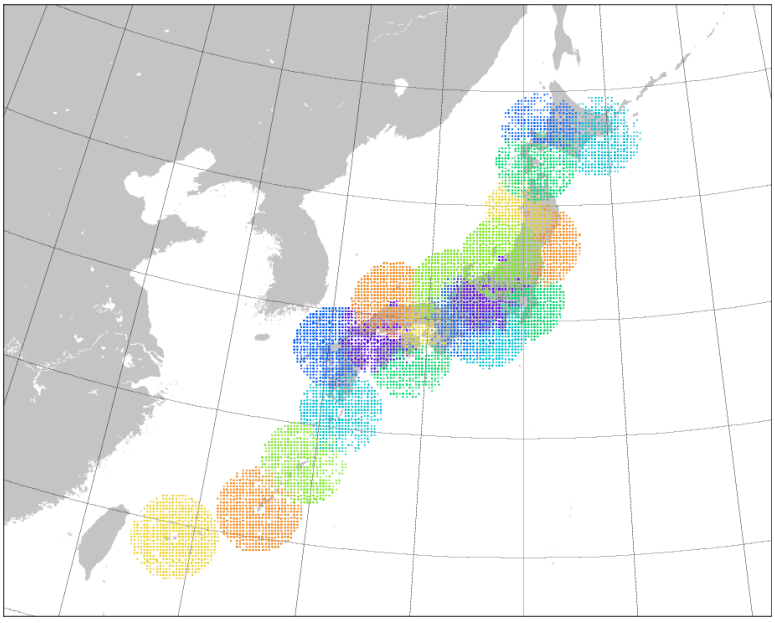

Figure 1. Area covered by retrieved RH data from JMA's C-band radar network

[1] ikuta@met.kishou.go.jp

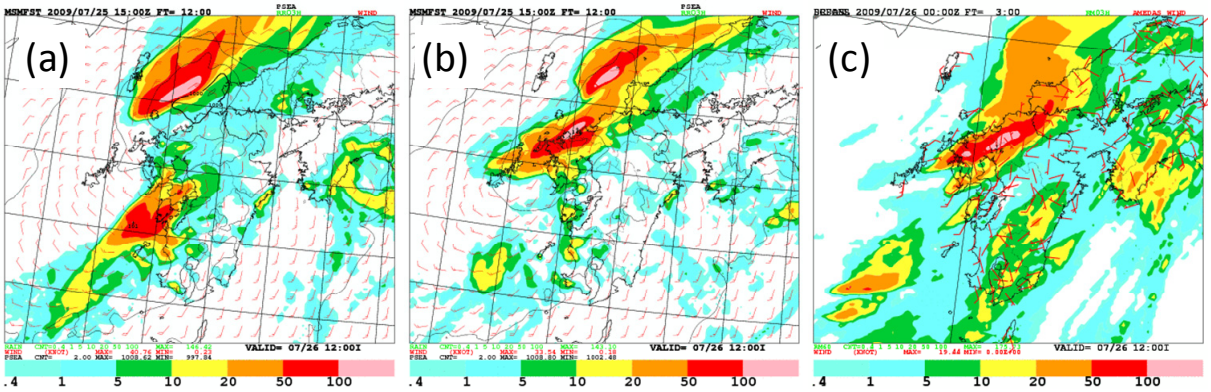

Figure 2. 3-hour cumulative precipitation at a forecast time of 12 hours: (a) control experiment, (b) test experiment, and (c) observation

**Reference**

Ikuta, Y. and Y. Honda, 2011: Development of 1D+4DVAR data assimilation of radar reflectivity in JNoVA. *CAS/JSC WGNE Res. Activ. Atmos. Oceanic Modell.,* **41**, 01.09 – 01.10.

# Simplified basic state update in the JMA global 4D-Var

Toshiyuki Ishibashi
Meteorological Research Institute, Japan Meteorological Agency
E-mail: ishibasi@mri-jma.go.jp

## 1. Introduction

Remote sensing observations are one of the main information sources in atmospheric analyses. Furthermore, cloud and rain affected remote sensing observations may bring significant improvements of analysis and forecast accuracy in near future. Nonlinearity of observation operators of these data is stronger than that of conventional direct observations. Therefore, data assimilation systems (DASs) have to treat such nonlinearity.

Analyses of the atmosphere based on variational schemes are executed with optimization algorithms using gradients of a cost function. Therefore, it is needed that nonlinearity of observation operators is weak. If tangent linear approximation of observation operators around a basic state is valid, this condition is satisfied and operational DASs are able to be stable and keep high accuracy.

In this paper, we describe results of cycle experiments of a simplified basic state update scheme.

## 2. Method

To update a basic state, we also need to update departure values, differences between observations and guesses, and computational costs of such update using an outer forecast model are not small. However, if we explicitly use an assumption for representative errors of observations and guesses, which is used implicitly in an incremental system, the rerun of outer model is not needed (Ishibashi 2011). Therefore, we can construct a basic state update scheme without outer model rerun, and we call this formulation a simplified basic state update.

The simplified basic state update scheme has been tested in a few single analysis and forecast experiment, and these experimental results show that the scheme can derive more information from relatively strong nonlinear observations (radiances, GPS-ROs, and humidity observations), and forecast accuracy is improved (Ishibashi 2011).

## 3. Experimental design

We executed two analysis and forecast cycles TEST and CNTL, here, TEST is a cycle with the simplified basic state update scheme, and CNTL with original scheme (no basic state update). The experimental system is a low resolution version of the JMA global NWP system, which has same spec with the JMA operational system except for horizontal grid resolution is about 60 km (operational is 20 km). Analyses were run from Jul 20 to Sep 9 (52 days), and 9 days forecasts are executed in August in 2009.

## 4. Results

First, we compare analysis fields of TEST and CNTL. Figure 1 shows differences of water vapor fields between these experiments in monthly average. We can find TEST has more precipitable water than CNTL in Tropics, and water vapor mixing ratio of TEST is larger in mid troposphere and smaller in low troposphere than those of CNTL (Figure 1(b)). Figure 1(c) shows validation of these changes using radio sonde observations as truth. We can find TEST reduces dry biases in mid troposphere and wet biases in low troposphere, therefore we can guess these changes in water vapor fields are adequate.

Secondly, we compare forecast fields of TEST and CNTL. Figure 2 shows normalized differences of root mean squared errors of forecasts between these experiments. We can find when we use radio sonde observations as truth, TEST has smaller RMSEs than CNTL in average. While, when we use initial fields as truth, TEST has larger RMSEs before 2 days in NH and SH, and almost all days in TP. To validate this contradiction in these two verifications, we show third verification, which used radiance data as truth (Figure 3). The figure shows that TEST has smaller RMSEs in average. Therefore, we can guess that the discrepancy comes from methodological problem of the verification using initial fields. Since the verification using initial fields assumes enough error growth against analysis errors, it cannot makes adequate verification when analysis biases are different in two experiments and those biases come from forecast model biases, in first few days and weak error growth area.

To see existence of forecast model bias, Figure 4 is monthly averages of 24 hours precipitation forecasts at a valid time of 24 hours and 72 hours. We find precipitation decreases when forecast time increases in tropical west pacific region. This and the dry (wet) biases in mid (low) troposphere shown in Figure 1(c), imply the forecast model cannot keep water vapor in the atmosphere, and drops them as precipitation during first few days. Therefore, we can see that this model bias makes the verification using initial fields inadequate.

However, there is another aspect of this model bias. Figure 4 shows zonal mean 24 hours precipitation of the first forecast day, we find TEST is larger precipitation. This is results of the wrong model response to the mid troposphere humidity increase in TEST, and this process may partly degrade forecast accuracy of TEST.

## 5. Future work

We plan two works. The first is to clarify conditions that the verification using initial fields is valid or invalid. The second is to treat forecast model biases in the DAS.

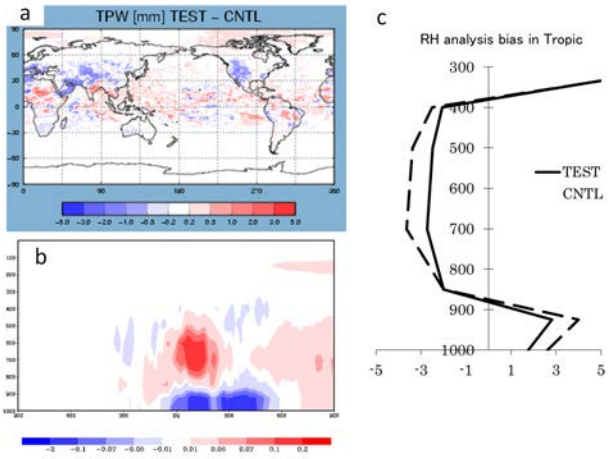


Figure 1. Analysis field differences between TEST and CNTL. The panel (a) is differences (TEST minus CNTL)of precipitable water, and the panel (b) is those of zonal mean water vapor mixing ratio, and the panel (c) is relative humidity biases against radio sonde observations.

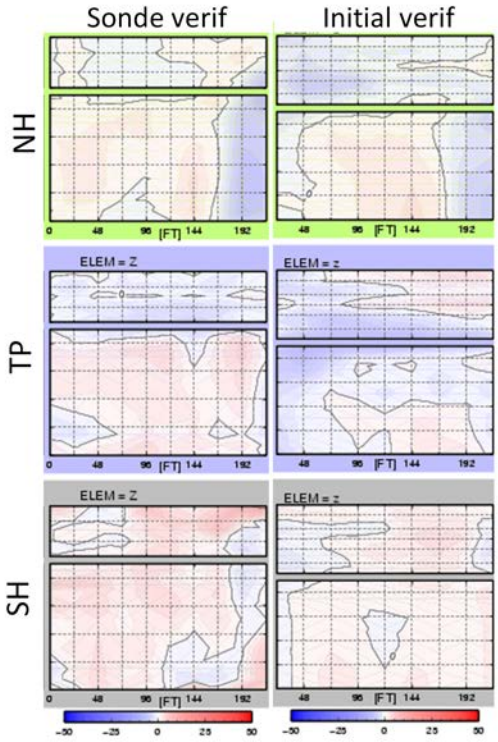


Figure 2. Differences of forecast RMSEs between TEST and CNTL (CNTL minus TEST) normalized by RMSEs. The left column is verification using radio sonde as truth, and the right using initial field for each region, the Northern hemisphere (NH), the Tropics (TP), and the Southern hemisphere (SH). TEST decrease (increase) forecast errors in red (blue) regions area. The horizontal axis is forecast times and the vertical axis is pressure height (surface to stratosphere)

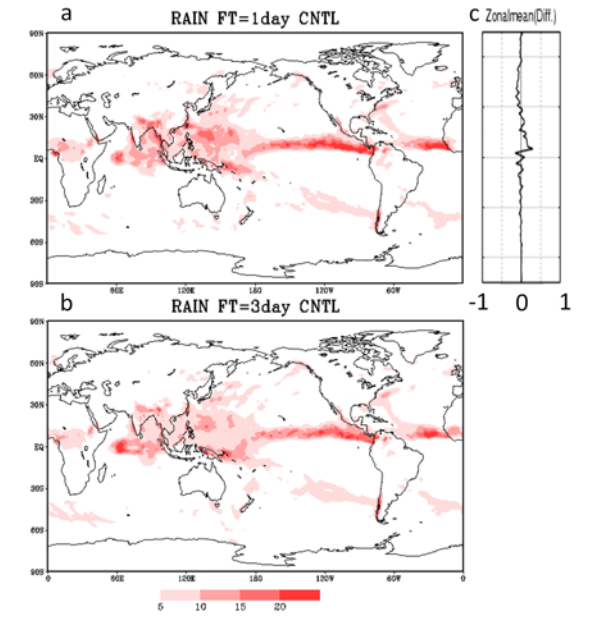


Figure 4. Rain forecast dependencies on forecast valid times and forecast rain differences. The panel (a) and (b) are 1 day precipitation at valid time of forecast day 1 and day 2, respectively. The panel (c) is differences of 1 day forecasted rain between TEST and CNTL (TEST minus CNTL).

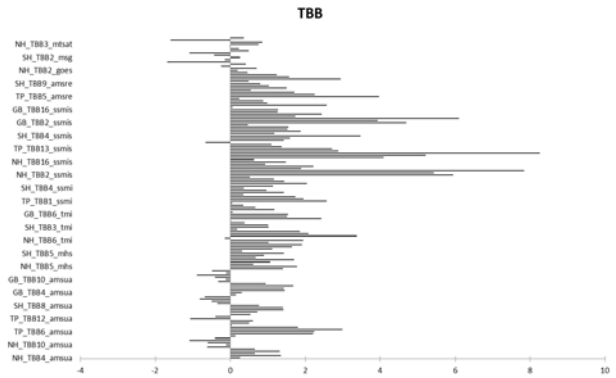


Figure 3. Differences of standard deviations of departure values of radiance data. Plus (minus) means TEST decreases (increases) errors.

# A new inner model with a higher horizontal resolution (TL319) in JMA's Global 4D-Var data assimilation system

Takashi Kadowaki and Koichi Yoshimoto
Numerical Prediction Division, Japan Meteorological Agency
1-3-4 Otemachi, Chiyoda-ku, Tokyo 100-8122, Japan
(e-mail: tkadowak@naps.kishou.go.jp, k-yoshimoto@met.kishou.go.jp)

Since February 2005, a four-dimensional variational (4D-Var) data assimilation system has been employed for atmospheric analysis to provide initial conditions for JMA's Global Spectral Model (GSM) (Kadowaki 2005; JMA 2007). In this system, analysis increments are calculated using an inner model with a horizontal resolution lower than that of the GSM due to the limitations of available computational resources. The resolution of the inner model was originally configured as T63L40, and was enhanced to T106L40 in March 2006 (Narui 2006), then to T159L60 in November 2007. A reduction in the 4D-Var system's calculation time was required in order to allow further enhancement of the inner model's resolution from T159L60, which was still insufficient for the GSM's TL959L60 resolution. In the inner model, a Eulerian advection scheme and standard Gaussian grids were used. A semi-Lagrangian advection scheme and adaptive (reduced) Gaussian grids (Miyamoto 2009), both of which have been used in the GSM since August 2008, were also introduced into the 4D-Var system (Kadowaki 2009). This introduction was able to successfully enhance the inner model's resolution to TL319L60 in October 2011 while requiring less additional computational power. At the same time, the background and observational error statistics used in the 4D-Var system were also recalculated.

Observation errors for the new 4D-Var system were estimated through a statistical study based on the work of Desroziers et al. (2005). The statistical period covered the two months of August and January 2010. Observation errors for conventional and satellite observations were calculated from the covariance of the differences between the observations and first guesses and those between the observations and analyses. The observation errors were also adjusted manually through forecast-analysis cycle experiments. The results are shown in Fig. 1. The estimated observation errors for temperature and brightness temperature are smaller than the previous ones, while those for wind components become larger above the stratosphere.

In order to evaluate the performance of the new system, forecast-analysis cycle experiments were performed for the two months of January and August 2010. Nine-day forecasts were made once a day based on 12 UTC initial conditions throughout the experimental period. Improvements on 500-hPa geopotential height forecasts were found in comparison with the previous system, mainly in the Northern Hemisphere (Fig. 2). Figure 3 shows the track forecast errors for seven typhoons observed from 01 August, 2010, to 09 September, 2010. The values for the new system are almost the same as those for the previous system, although in some cases the new system better represented the atmospheric structure around typhoons, as shown in Fig. 4.

References:

Desroziers, G., L. Berre, B. Chapnik and P. Poli, 2005: Diagnosis of observation, background and analysis-error statistics in observation space. Quart. J. Roy. Meteor. Soc., **131**, 3,385 – 3,396.

JMA, 2007: Outline of the operational numerical weather prediction at the Japan Meteorological Agency. Appendix to WMO Numerical Weather Prediction Progress Report. Japan Meteorological Agency, Tokyo, Japan. Available online at http://www.jma.go.jp/jma/jma-eng/jma-center/nwp/outline-nwp/index.htm.

Kadowaki, T., 2005: A 4-dimensional variational assimilation system for the JMA Global Spectrum Model.

CAS/JSC WGNE Research Activities in Atmospheric and Oceanic Modelling, **34**, 1 – 17.

Kadowaki, T., 2009: Development of a Semi-Lagrangian Inner Model for Improving the Inner Resolution of the JMA Global Analysis System. CAS/JSC WGNE Research Activities in Atmospheric and Oceanic Modelling, **39**, 1 – 17.

Miyamoto, K., 2009: Recent Improvements to the JMA Global NWP Model. CAS/JSC WGNE Research Activities in Atmospheric and Oceanic Modelling, **39**, 6 – 09.

Narui, A., 2006: Changing the Resolution of the Inner Loop of Global 4D-Var at JMA. CAS/JSC WGNE Research Activities in Atmospheric and Oceanic Modelling, **35**, 1 – 23.

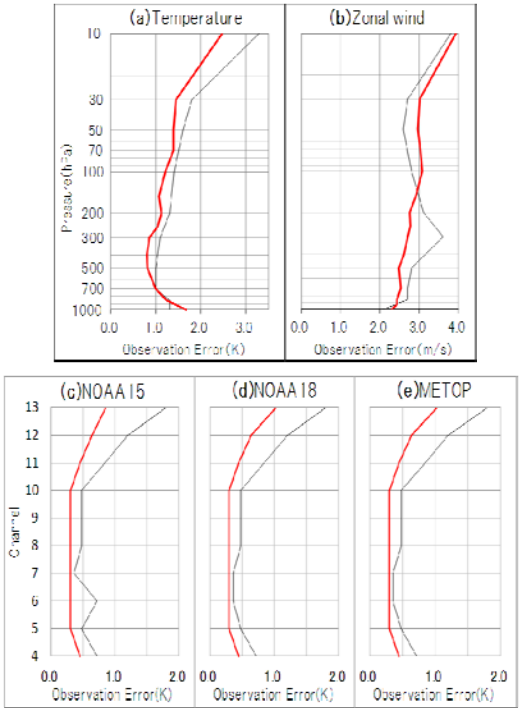


Fig. 1: Observation errors for conventional and satellite brightness temperatures. (a) Temperature, (b) Zonal wind, AMSU-A aboard (c) NOAA15, (d) NOAA18, and (e) METOP. The statistical period covers the two months of August and January 2010. The red and black lines show observation errors for the new and previous systems, respectively.

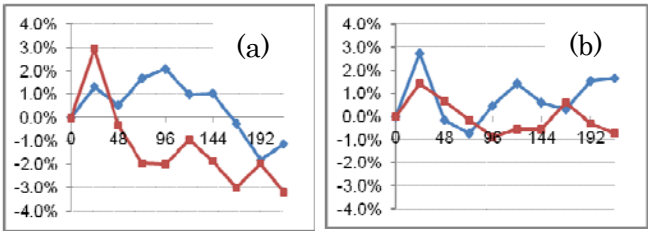


Fig. 2: Improvement rates (%) of the RMSE in 500hPa height for the new system against the previous system. The horizontal axis represents forecast hours. Positive values indicate improved scores. The blue and red lines represent the northern and southern hemispheres, respectively. (a) January 2010, and (b) August 2010.

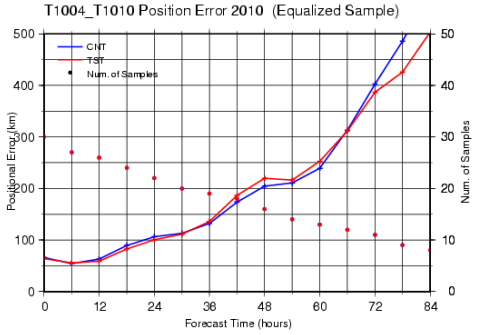


Fig. 3: Track forecast errors for seven typhoons observed from 01 August, 2010, to 09 September, 2010. The red and blue lines represent the new and previous systems, respectively.

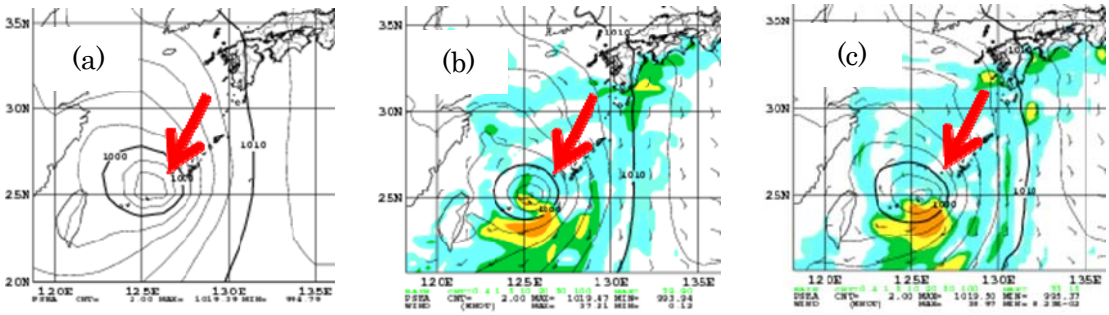


Fig. 4: Horizontal distributions of mean sea level pressure (contours) in hPa and precipitation (shading) in mm/3h. (a) Analysis and 12-hour forecast with (b) the previous system and (c) the new system.

# Assimilation experiments involving surface-sensitive microwave radiances in JMA's global data assimilation system

Masahiro Kazumori
Numerical Prediction Division, Japan Meteorological Agency
E-mail: kazumori@met.kishou.go.jp

The Japan Meteorological Agency (JMA) operates a global model for short- to medium-range weather forecasting, and a four-dimensional variational method is employed to produce the initial conditions for such forecasts. Since 2003, satellite-observed radiance data have been assimilated using a fast radiative transfer model (RTTOV) [1] in the global data assimilation system. Although data from observations over oceans are intensively used, current use over land is limited to channels that are not sensitive to surface conditions. Recent studies ([2], [3]) have suggested the possibility of using information from surface-sensitive microwave radiances if improved land surface emissivity and land surface temperature estimates are used together in radiative transfer calculation. The goal of this research was to improve global forecast skill using lower tropospheric microwave channels over land in data assimilation.

In JMA's current radiative transfer calculation for the satellite data assimilation, land surface emissivity is set to a fixed value and the atmospheric temperature at the lowest model level from the short-range global forecast is used as a substitute for land surface temperature. In order to assimilate surface-sensitive microwave radiances from various microwave radiometers, climatological land surface emissivity values supplied with RTTOV-10 codes were employed in assimilation experiments, and hourly land surface temperature data from JMA's global land surface model were also used. Although observation errors of AMSU-A channel 6 over land were inflated in the current system due to inappropriate land surface emissivity usage, the utilization of climatological land surface emissivity values makes it possible to reduce the inflation factor. The hourly land surface temperature was used as a predictor in the variational bias correction of radiance data. With these improvements, the lower tropospheric channels of MHS (channel 3, 4 and 5) over land were newly incorporated into the assimilation experiments. A one-month experiment for August 2010 was run using the low-resolution version (TL319L60) of JMA's global data assimilation system in its July 2011 operational version. The control experiment was performed with the same configuration as the operational one. In the test experiment, the modifications were applied for the control run.

Impacts of MHS assimilation over land were seen in desert areas with an increase in total column water vapor (TCWV) (Figure 1(a)). The increased values were consistent with data from ground-based GPS integrated water vapor observation (Figure 1 (b) and (c)) and TCWV values retrieved from MERIS [4] on ENVISAT (Figure 2) in the desert area. A reduction of O – B departure during the assimilation experiment period was also found for AMSU-A channel 6, and improvement of short-range forecast errors for the temperature at 850 hPa was seen globally (not shown here).

Assimilation of MHS radiance data over land with the emissivity atlas and hourly surface temperature brought a forecast improvement in JMA's global data assimilation system. Plans are now being made to extend the use of climatological surface emissivity values for other microwave radiance data (such as SSMIS, AMSR-E and AMSR2 on GCOM-W1). Further, in order to obtain more realistic information from measurements, dynamical estimation of land surface emissivity value and/or land surface temperatures in the data assimilation system are planned.

## References


[1] Saunders, R. W., 2008: RTTOV-9 Science and Validation Report. EUMETSAT, pp. 74.

[2] Karbou, F., E. Gerard and F. Rabier, 2006: Microwave land emissivity and skin temperature for AMSU-A and -B assimilation over land. *Quart. J. Roy. Meteor. Soc.*, **132**, 2333 – 2355.

[3] Karbou, F., E. Gerard and F. Rabier, 2010: Global 4DVAR assimilation and forecast experiments using AMSU observations over land. Part I: Impacts of various land surface emissivity parameterizations. *Wea. Forecasting*, **25**, 5 – 19.

[4] ESA, 2006: MERIS Product Handbook. European Space Agency Issue **2.1**, 24th October 2006.


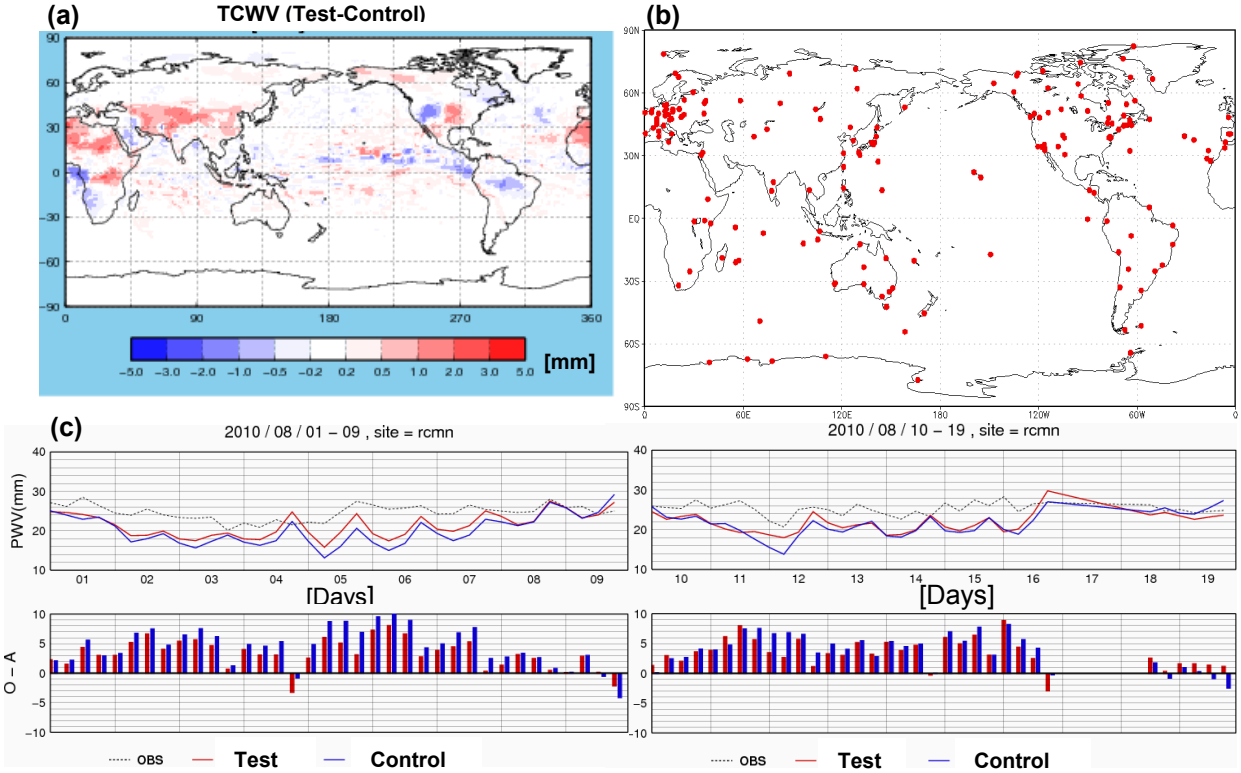


Figure 1 (a) Map showing monthly mean differences between TCWV analysis from the test and control experiments for August 2010. (b) Map showing available global GPS observation locations for August 2010. The GPS location selected for verification is indicated with a black arrow. (c) Six-hourly TCWV based on GPS (black dotted line) and TCWV analysis from the test run (red line) and the control run (blue line). The vertical bars in the lower panels indicate the difference between GPS TCWV and TCWV analysis values.

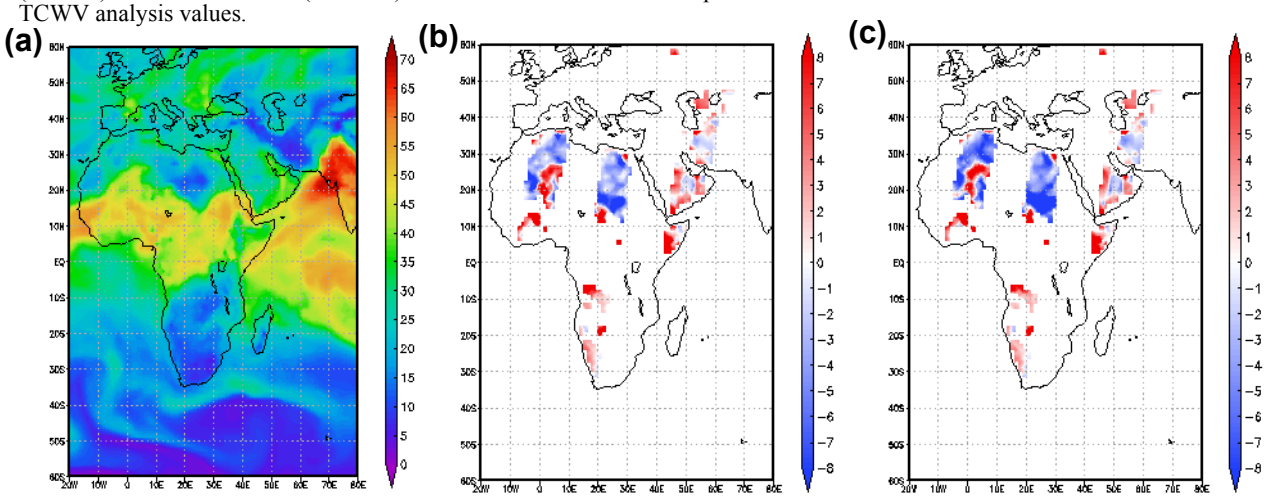


Figure 2 (a) The TCWV field analyzed in the test experiment at 12 UTC on August 1, 2010. (b) Differences of TCWV as analyzed in the test experiment and those from the MERIS TCWV product. (c) As per (b), but for the control experiment. The units are mm.

# Initial assessment of FY-3A microwave temperature sounder radiance data in JMA's global data assimilation system

Masahiro Kazumori and Hidehiko Murata
Numerical Prediction Division, Japan Meteorological Agency
E-mail: kazumori@met.kishou.go.jp, hidehiko.murata@met.kishou.go.jp

Observations from microwave radiometers currently play an important role in data assimilation for Numerical Weather Prediction (NWP). Microwave observations contain information on atmospheric temperature and moisture under all weather conditions. The Advanced Microwave Sounding Unit- A (AMSU-A) is a temperature sounding instrument, and the assimilation of radiance data has a large positive impact on NWP. Accordingly, such data have been widely used at many NWP centers to produce initial conditions for prediction. These instruments are currently aboard NOAA (NOAA-15, 16, 18, and 19), Aqua and Metop satellites.

China's FY-3A satellite was launched in May 2008 and is also equipped with a microwave temperature sounding instrument (MWTS). The instrument's design is similar to that of AMSU-A. It uses four channels for atmospheric temperature sounding (MWTS channels 1, 2, 3 and 4 correspond to AMSU-A channels 3, 5, 7 and 9, respectively). In previous studies ([1], [2]), the quality of FY-3A MWTS radiance data was closely investigated and related issues were pointed out (i.e., pass-band shift of the central frequency and radiometer non-linearity). These studies proposed a method to correct such effects in the brightness temperature calibration process and in radiative transfer calculation. In our study, FY-3A MWTS radiance data after the calibration update by the National Satellite and Meteorological Center (NSMC) of the China Meteorological Administration (CMA) were used. For the fast radiative transfer model, RTTOV-10 [3] with a modified coefficient for FY-3A MWTS on the pass-band shift effect was utilized. In the initial assessment of FY-3A MWTS in JMA, the latest low-resolution version (TL319L60) of JMA's global data assimilation system was employed for the preliminary test. FY-3A MWTS data from July 20 to September 9, 2011, were obtained from the Fengyun Satellite Data Center (http://fy3.satellite.cma.gov.cn/arssen/) in non-real time for the assimilation experiment. FY-3A MWTS channels 2 and 3 were assimilated, and channel 1 was used to screen out cloud-contaminated data. The control run had the same configuration as JMA's operational global data assimilation system as of September 2011 except for the outer and inner model's horizontal resolution. In the test run, FY-3A MWTS data were incorporated into the control run.

The results of the quality check (O – B (Observed minus Background) departure statistics) in the JMA system indicated that the quality of FY-3A MWTS data is similar to or slightly better than that of AMSU-A (e. g., Metop and NOAA-18) [Figure 1]. In the data assimilation experiment, similar quality control and predictors of variational bias correction were applied for FY-3A MWTS. The thinning distance for MWTS was set as 160km, whereas that of AMSU-A was 250km.

From the data assimilation experiment, consistent temperature forecast improvements were confirmed in verification against radiosonde observation and initial field verification for the Southern Hemisphere [Figure 2]. The impacts for the Northern Hemisphere and the Tropics were almost neutral. The results obtained here were encouraging, and suggest that the improvement of temperature analysis with FY-3A MWTS data assimilation can lead to temperature forecast improvements like AMSU-A data assimilation.

To enable operational use of FY-3A/B MWTS data in JMA's data assimilation system, it is necessary to obtain data in real time and to perform further investigation on the assimilation impact of FY-3A/B.

## References


[1] Lu, Q., Bell, W., Bauer, P., Bormann, N. Peubey, C. 2011. An evaluation of FY-3A satellite data for numerical weather prediction. *Q. J. R. Meteorol. Soc.* **137**: 1298 – 1311. DOI:10.1002/qj.834.

[2] Lu, Q., Bell, W., Bauer, P., Bormann, N. Peubey, C. 2011. Characterizing theFY-3A Microwave Temperature Sounder Using the ECMWF Model. *J. Atmos. Ocean. Tech.* **28** 1373 – 1389. DOI: 10.1175/JTECH-D-10-05008.1.

[3] Saunders, R. et al., 2012: RTTOV-10 Science and Validation Report. EUMETSAT, pp. 31


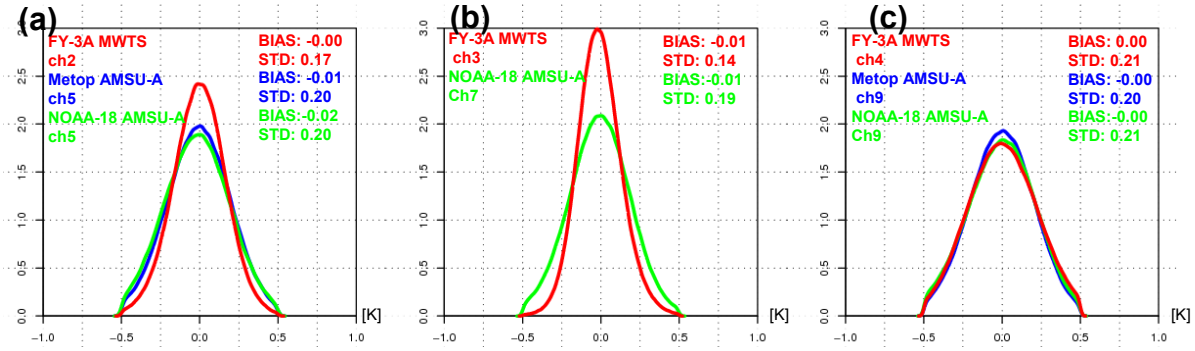


Figure 1 Comparison of O − B departure normalized histograms (a) FY-3A MWTS channel 2 (red), Metop AMSU-A channel 5 (blue) and NOAA-18 AMSU-A (green), (b) FY-3A MWTS channel 3 (red), NOAA-18 AMSU-A channel 7 (green); and (c) FY-3A MWTS channel 4 (red), Metop AMSU-A channel 9 (blue) and NOAA-18 AMSU-A channel 9 (green). The statistics were calculated with bias-corrected O − B values from a one-month (August 2011) data set.

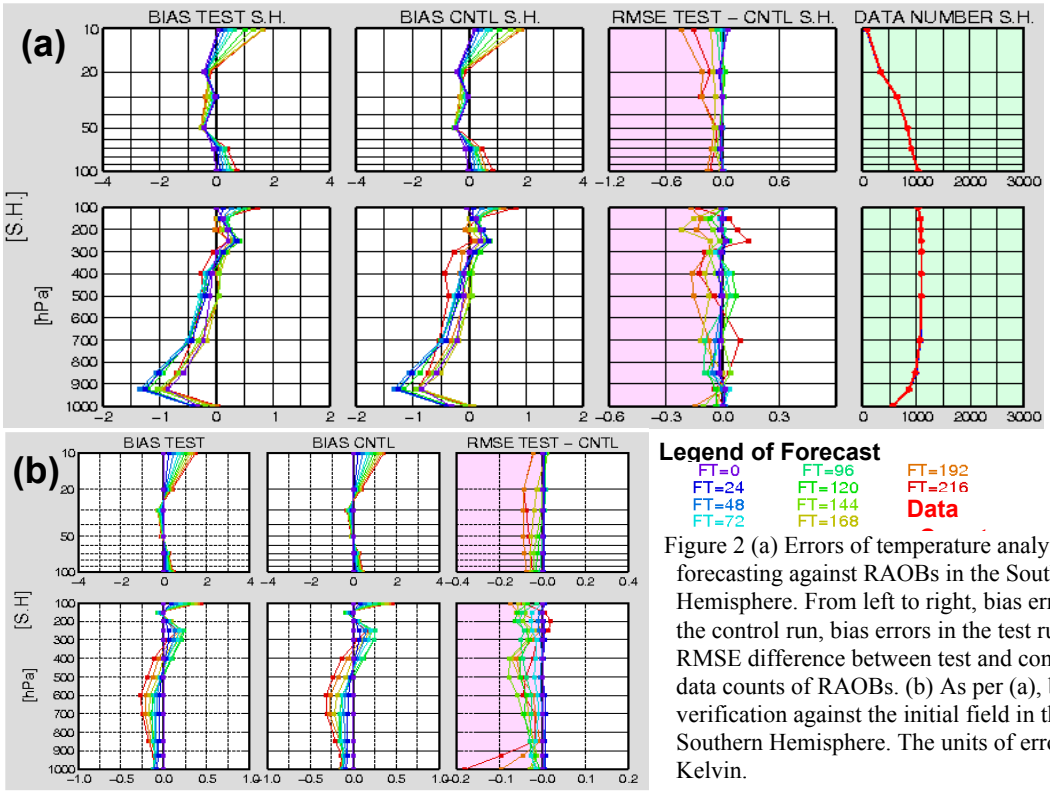


Figure 2 (a) Errors of temperature analysis and forecasting against RAOBs in the Southern Hemisphere. From left to right, bias errors in the control run, bias errors in the test run, RMSE difference between test and control, and data counts of RAOBs. (b) As per (a), but for verification against the initial field in the Southern Hemisphere. The units of error are Kelvin.

# Construction of Mesoscale LETKF Data Assimilation Experiment System

**Tohru KURODA**

*Japan Agency for Marine-Earth Science and Technology, Yokohama, Kanagawa, 236-0001, Japan;*

*tkuroda@jamstec.go.jp*

**Tadashi FUJITA**

*Numerical Prediction Division, Japan Meteorological Agency, Chiyoda-ku, Tokyo 100-8122, Japan;*

**Hiromu SEKO and Kazuo SAITO**

*Meteorological Research Institute, Tsukuba, Ibaraki 305-0052, Japan;*

A development of a mesoscale LETKF (Local Ensemble Transform Kalman Filter) data assimilation system is ongoing in the field 3 task "Projection of Planet Earth Variations for Mitigating Natural Disasters" of the SPIRE (Strategic Programs for Innovative Research) project supported by the Ministry of Education, Culture, Sports, Science and Technology, aiming achievements by means of the high performance of K computer. The system consists of assimilation cycles each of which has ensemble forecast and analysis parts, and is considered to be suitable for the parallel computer since its ensemble forecast can be executed as concurrent jobs, and the LETKF analysis is a well parallelized scheme. We plan to apply this system to obtain precise analysis that enables a forecast on severe whether such as a localized torrential downpour.

This system applies the Japan Meteorological Agency (JMA) Nonhydrostatic Model (NHM) as the forecast model, and uses an LETKF analysis which is based on that of Miyoshi and Aranami (2006). The ensemble forecast with the size of 40 members and with a 10km horizontal resolution is conducted in an assimilation cycle with a six hour time window, and a control forecast runs at the same time. Perturbations for initial values of ensemble forecast in the first analysis cycle and that for lateral boundary in the every cycle are given by the perturbation of the JMA weekly global ensemble forecast. Diagram of data assimilation cycle is shown in Figure 1 (T. Fujita, NPD/JMA, 2011).

Six hourly cycle data assimilation is performed with one hour slots in the way of 4D-LETKF. After the LETKF analysis, another analysis on the initial value of the control forecast is executed applying a Kalman gain obtained in the LETKF procedure, and then an outer-loop forecast is executed using the analysis as the initial value.

A final value of the outer-loop 6 hour forecast is used as an initial value of control forecast, and contributes to initial value of ensemble forecast in the subsequent cycle.

Adaptive inflation (Miyoshi 2010) is applied in addition to multiplicative inflation. Horizontal and vertical localizations are implemented, too. Observations on surface, upper layer, aviation, doppler radar, wind profile, satellite wind, satellite brightness temperature can be assimilated by this system. Quality control procedure ported from the JMA operational system (JMA, 2007, Kazumori 2010) is applied on these observations to choose data to be assimilated.

Figure 2 shows a performance of LETKF for the spread of temperature and east-west wind component fields at the altitude of about 5500 m. We can see a spread in the analysis fields which is smaller than that in the guess fields around land area where observation is comparatively dense. After the LETKF analysis, an 6 hour forecast of outer loop gives a rainfall rate as shown in Fig. 3.

We will apply this system to cases with more spatiotemporal resolution in order to solve storm scale severe phenomena although it requires so huge calculation cost as to need to use K computer. We continue to develop this system with investigating appropriate parameter which concerned with covariance error statistics, localization and inflation, and with improving the computational performance.

**References**

[1] Fujita, T., 2011: MSM-LETKF. Annual Report of Numerical Prediction Division, **57**, 138-143. (in Japanese).

[2] Japan Meteorological Agency, 2007: Outline of the operational numerical weather prediction at the Japan Meteorological Agency, available from the Japan Meteorological Agency, 194pp.

[3] Kazumori, M., 2011: Operational Use of Satellite Radiance in JMA Mesoscale Analysis, CAS/JSC WGNE Research Activities in Atmospheric and Oceanic Modeling, **41**, 1.17-1.18

[4] Miyoshi, T., and K. Aranami, 2006: Applying a Four-dimensional Local Ensemble Transform Kalman Filter (4D-LETKF) to the JMA Nonhydrostatic Model (NHM). *SOLA*, **2**, 128-131.

[5] Miyoshi, T., 2010: The Gaussian Approach to Adaptive Covariance Inflation and Its Implementation with the Local Ensemble Transform Kalman Filter, *Mon. Wea. Rev.*, **139**, 1519–1535.

[6] Saito, K., J. Ishida, K. Aranami, T. Hara, T. Segawa, M. Narita and Y. Honda, 2007: Nonhydrostatic atmospheric models and operational development at JMA. J. Meteor. Soc. Japan, **85B**, 271-304.

[7] Saito, K., H. Seko, T.Kuroda, T. Fujita, T. Kawabata, K. Aonashi, and T. Tsuyuki, 2011: Next generation supercomputer project toward cloud resolving NWP. CAS/JSC WGNE Res. Activ. Atmos. Oceanic Modell, **41**, 5.19-5.20.

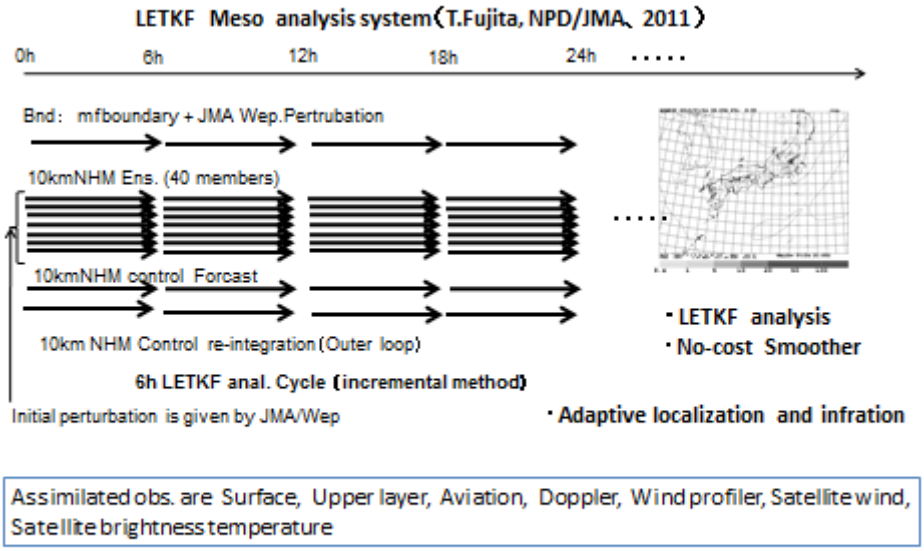


**Fig. 1.** Data Assimilation Cycles.

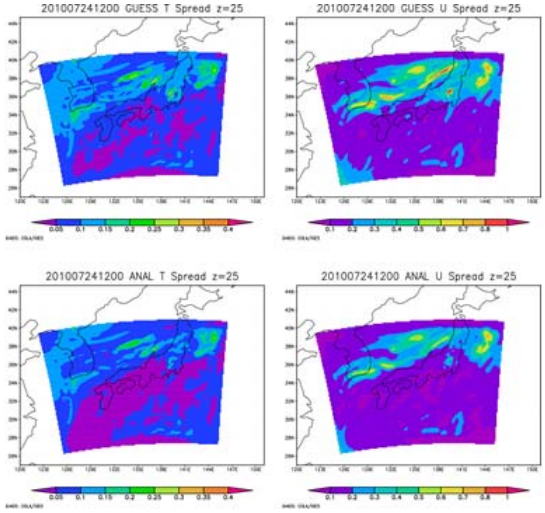


**Fig. 2.** Spreads on guess by ensemble forecast and on analysis obtained by LETKF analysis.

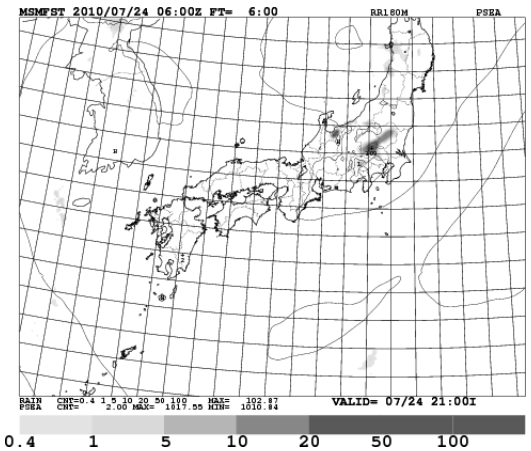


**Fig. 3.** Rainfall rate given by outer loop.

# Forecast sensitivity to observations at Météo-France
# Application to GPS radio-occultation data

**Nathalie Saint-Ramond, Alexis Doerenbecher, Florence Rabier,**
**Vincent Guidard, Nadia Fourrié**

**CNRM-GAME, Météo-France and CNRS**
**42 av Coriolis**
**31057 Toulouse, France**
**nathalie.saint-ramond@meteo.fr**

The 4DVAR system used at METEO-FRANCE processes and assimilates a large amount of satellite and ground based observations. Such a large number of observations needs to be monitored to evaluate their impact on forecast skill. In order to improve weather forecasts and assimilations, the capability to compute the forecast sensitivity to observations has been implemented at Météo-France. This technique (Langland and Baker, 2004) is now commonly used as a complement to data denial experiments. The code implemented in our global model ARPEGE has been developed at ECMWF by C. Cardinali and M. Fisher.

To compute the observation impact, we define a cost function J representing the forecast error. Here, J is the three dimension integrated dry total energy of the difference between the 24 hour forecast and a reference state (e. g. verifying analysis) computed over the globe. The forecast sensitivity to observations calculation requires the adjoint of the forecast model and the assimilation system. In practice, the linear estimate of the forecast impact (deltaJ) calls for a second order approximation (Errico, 2007). It is then computed using both trajectories from analysis and background as shown in Fig.1.

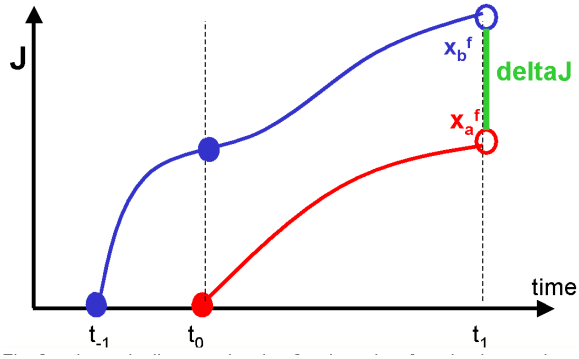


*Fig. 1: schematic diagram showing 2 trajectories from background (blue), and analysis (red). deltaJ appears in green.*

A forecast impact experiment has been conducted over the period going from December 2010 to mid January 2011. Fig.2a shows the results for observations assimilated in ARPEGE parted by observation group. AMSU-A and IASI have the biggest impact on the forecast error reduction. Computation of the impact of the different channels of IASI shows that the nine water vapour channels reduce the forecast error. Among the other ones, the biggest impact comes from Temperature channel pointing the UTLS. As far as AMSU-A is concerned, channel 7 and 8 in the upper troposphere and channel 13 at the highest level have the biggest influence on the forecast error reduction. These two instruments also bring most observations. If we consider a single source of observation (Fig. 2b), ground observations from buoy and radiosondes are the more informative. Concerning individual satellite observation, the biggest impact comes from Atmospheric Motion Vectors and GPS radio-occultation data.

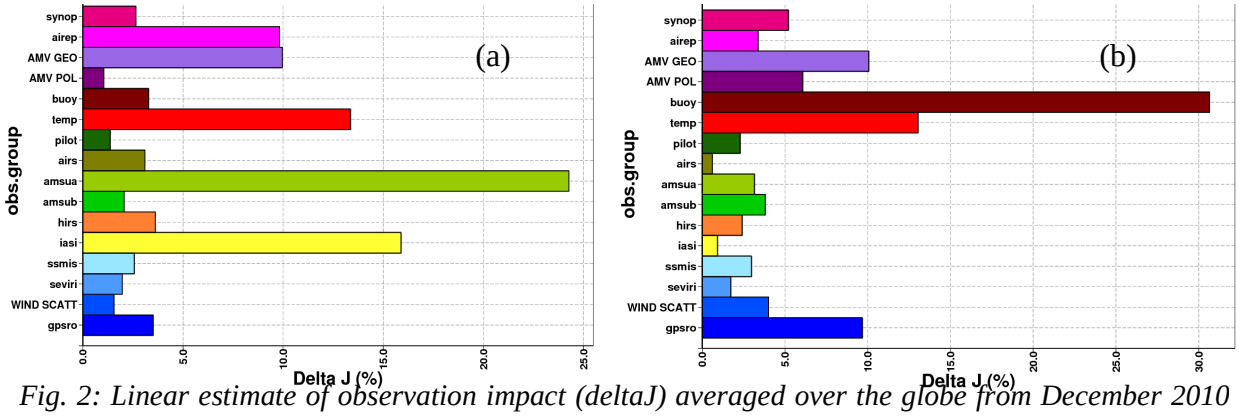


*Fig. 2: Linear estimate of observation impact (deltaJ) averaged over the globe from December 2010 to January 2011.(a) separated by observation group and (b) divided by observation number*

GPS RO data are assimilated in the global 4DVAR since September 2007. Bending angles are assimilated using 1D operator from GRAS-SAF. Data used in this experiment come from GRACE-A, FORMOSAT-3/COSMIC constellation and GRAS on Metop. Rising and setting occultations are used up to 36 km. A vertical thinning is operated to keep one datum per model vertical layer. These data have a good global coverage but their impact strongly depends on the altitude as shown in Fig.6a. The biggest impact is located in the UTLS and also at the highest assimilated levels. A bad impact is also noticeable at 29 km and 35 km high. Fig.6b show the impact on a grided map of data between 33 and 35 km. Even though the global impact is good, it is unevenly distributed at this height. The good values in the Northern hemisphere compensate for the bad ones over the tropics. This unevenness needs more investigation to know whether it comes from the model, J calculation, the weather regime or anything else.

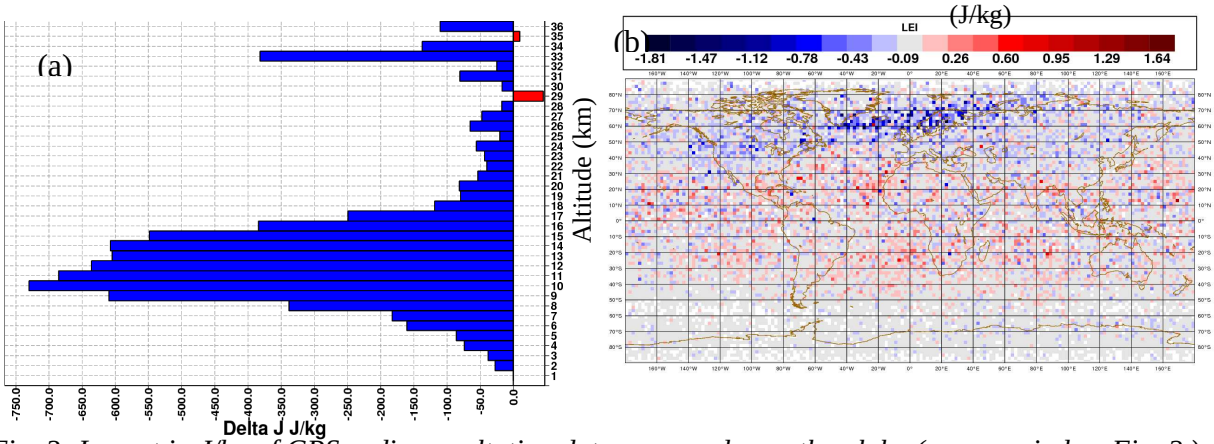


*Fig. 3: Impact in J/kg of GPS radio-occultation data averaged over the globe (same period as Fig. 2.) (a) depending on altitude in km and (b) 2°x2° grided averaged values between 33 and 35 km high.*

Accounting for the approximation made, the linear estimate can only be used to compute observation impact on a short range forecast, such as 24 hours and must be further investigated, using classical OSEs or on other periods for example.

## References:

Errico RM. 2007: Interpretations of an adjoint-derived observational impact measure. *Tellus* **59A**:273-273

Langland RH, Baker NL. 2004: Estimation of observation impact using the NRL atmospheric variational data assimilation adjoint system.*Tellus* **56A:**189-201

# GPS TPW Assimilation with the JMA Nonhydrostatic 4DVAR and Cloud Resolving Ensemble Forecast for the 2008 August Tokyo Metropolitan Area Local Heavy Rainfalls

Kazuo Saito[1], Yoshinori Shoji[1], Seiji Origuchi[1], Le Duc[2,1] and Hiromu Seko[1]
[1]Meteorological Research Institute, Tsukuba, Japan
[2]Japan Agency for Marine-Earth Science and Technology, Yokohama, Japan

On 5 August 2008, scattering local heavy rainfalls occurred various places over the Tokyo metropolitan area (Fig. 1a), and five drainage workers were claimed by abrupt flooding. The JMA's operational mesoscale model[1,2] of the day failed to predict occurrence of the local heavy rainfalls (Fig. 1b), which were given by deep convective cells developed on unstable atmospheric conditions without strong synoptic/orographic forcing. A 11-member mesoscale ensemble prediction with a horizontal resolution of 10 km was conducted using the JMA global EPS peruturbation as the initial and lateral boundary perturbations, but the associated intense rains exceeding 20 mm /3 hour were hardly predicted (Fig. 1c). A downscaling ensemble forecast experiment with a horizontal resolution of 2km was conducted using the 6 hour forecast of 10 km ensemble as the initial condition. Scattered intense rains were predicted in some members, but their distribution was not enough (Fig. 1d).

The total precipitatable water vapor (TPW) observed by GEONET (Fig. 2a) showed that the initial field of the operational MSM produced by the hydrostatic Meso-4DVAR (Fig. 2b) underestimated water vapor over the Tokyo metropolitan area. To modify the initial condition, a reanalysis data assimilation experiment was conducted with the JMA's nonhydrostatic 4DVAR (JNoVA[3]), where GPS TPW data from GEONET were assimilated 2.5 days with 3-hour data assimilation cycles. Figure 2c shows the modified TPW analysis obtained by JNoVA, where data thining of GPS observations was conducted with 15 km.

The 2 km downscale ensemble run from JNoVA analysis properly predicted the areas of scattering local heavy rains (Fig. 3). Threat scores (Fig. 4) and ROC area skill scores (Fig. 5) suggest that even in the ensemble prediction, accuracy of initial condition is critical to numerically predict small scale convective rains. Fractions skill scores[4] indicated the value of the cloud resolving ensemble forecast for such the unforced convective rain case.

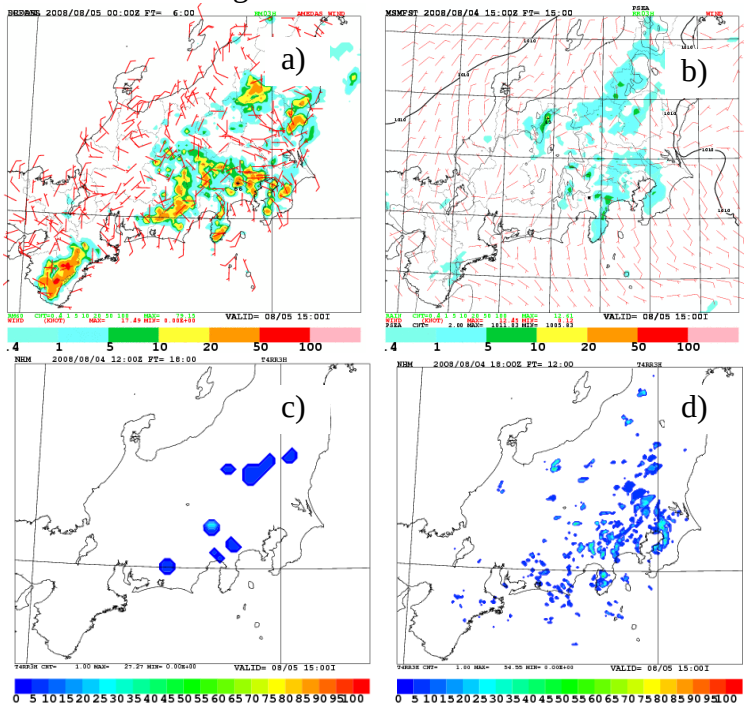


**Fig. 1.** a) Observed precipitation for 03-06 UTC, 5 August 2008. b) Forecast of the operational MSM. Initial time is 12 UTC 4, August 2008. c) Probability of precipitation over 20 mm / 3 hours by a 11-member EPS with a horizontal resolution of 10km. d) Same as in c) but downscale ensemble prediction of horizontal resolution of 2 km.

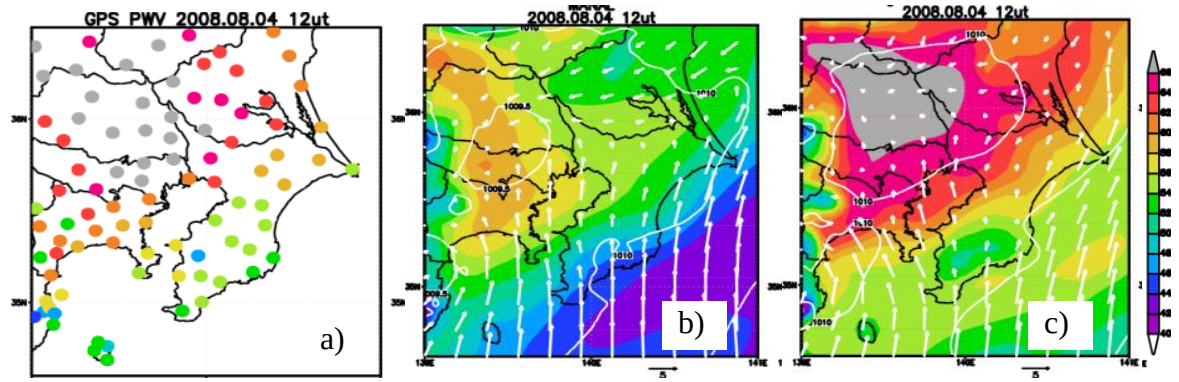


**Fig. 2.** a) TPW observed by GEONET at 12 UTC, 4 August 2008. b) TPW by Meso4DVAR analysis. c) Same as b) but TPW obtained by JNoVA analysis.

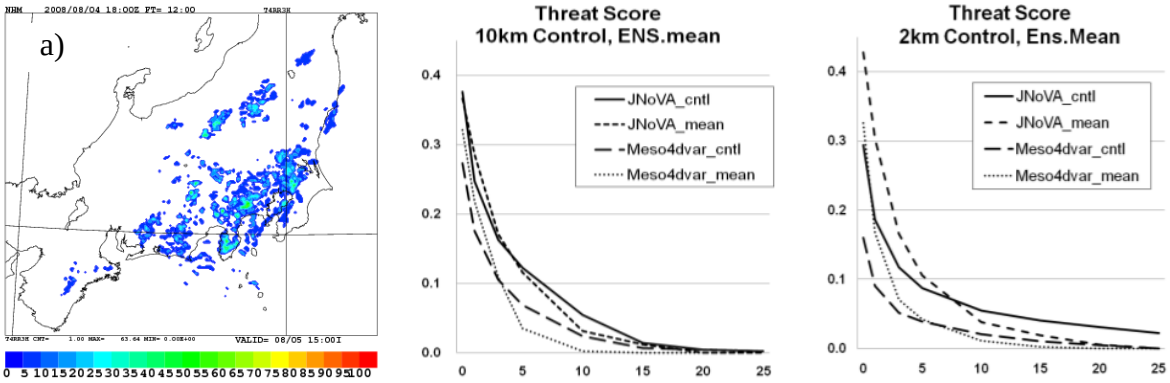


**Fig. 3.** (Left) Same as Fig. 1d, but EPS with JNoVA initial condition assimilating GPS TPW.
**Fig. 4.** (Right) a) Threat scores for 10 km EPS. b) Same as a) but 2 km EPS.

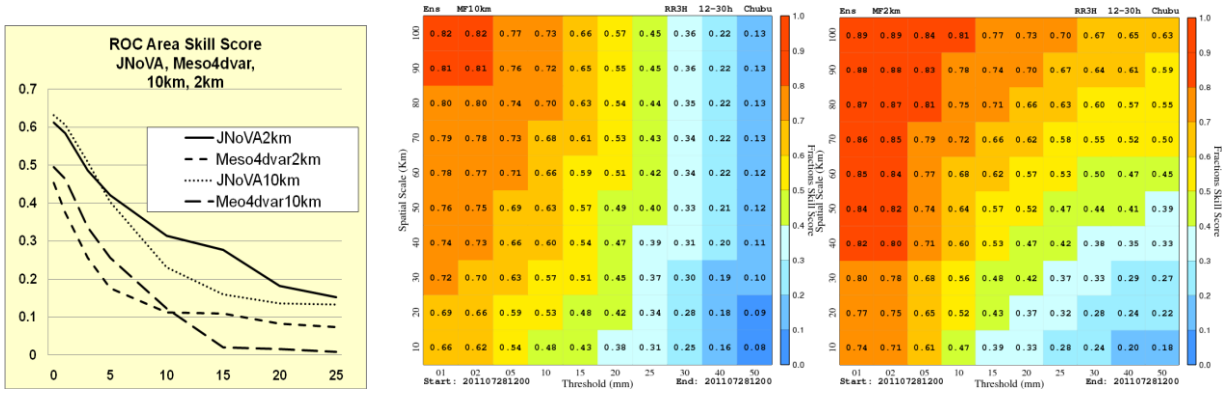


**Fig. 5.** (Left) ROC area skill scores by four ensemble prediction systems.
**Fig. 6.** Fractions skill score scale-intensity diagram for 10 km EPS (left) and 2km EPS (right).

## References


[1] Saito, K., J. Ishida, K. Aranami, T. Hara, T. Segawa, M. Narita and Y. Honda, 2007: Nonhydrostatic atmospheric models and operational development at JMA. *J. Meteor. Soc. Japan*, 85B, 271-304.

[2] Saito, K., 2012: The Japan Meteorological Agency nonhydrostatic model and its application to operation and research. *InTech* (in press).

[3] Honda, Y. and K. Sawada, 2008: A new 4D-Var for mesoscale analysis at the Japan Meteorological Agency. *CAS/JSC WGNE Res. Act. Atmos. Ocea. Model.*, **38**,.01.7-01.8.

[4] Roberts, N. M., and H. W. Lean, 2008: Scale-selective verification of rainfall accumulations from high-resolution forecasts of convective events. *Mon. Wea. Rev.*, **136**, 78–97.

# Observation System Simulation Experiments of Quasi-Zenith Satellite

Hiromu Seko (Meteorological Research Institute), Satoshi Kogure (JAXA)
and Toshitaka Tsuda (Kyoto University)

## 1. Introduction

Radio waves transmitted from GPS satellites are delayed before arriving at GPS receivers due to water vapor in the atmosphere. GPS-derived Precipitable Water Vapor (PWV) (water vapor amount above a GPS receiver), which is obtained from the delays of the radio waves, improves rainfall forecasts when this data is assimilated into initial conditions of numerical forecasts. However, GPS-derived PWV does not always express the water vapor amount in the zenith direction (Zenith Water Vapor (ZWV)) because GPS satellites positions are not static. If the PWV obtained by satellites that stay around zenith direction, such as the Quasi-Zenith Satellite (QZS), can be used in the assimilation, this PWV is expected to be closer to ZWV and to improve the rainfall forecast. QZS stays not only around the zenith direction but also at low-elevation angles for long periods. Because the low elevation data has the information of anisotropy of water vapor distribution (namely, water vapor amounts along slant paths (SWV) with low elevation angles have the information of directions where humid air exists), SWV is also expected to improve rainfall forecasts. In this study, the potential of QZS, whose position stays around the zenith direction and in low-level elevations for long periods, of the improvements on rainfall forecasts is investigated by the observation system simulation experiments (OSSE).

## 2. Outline of the observation system simulation experiments

In the observation system simulation experiments, artificial data is obtained from the outputs of numerical models in which the phenomenon of interest was well reproduced (Truth data). The truth-derived artificial data (hereinafter, truth-derived data) is then assimilated into the fields in which the phenomenon of interest was not reproduced (First guess data). The impacts of the truth-derived data are investigated by checking how it improves the fields. In this study, impacts of QZS data on the assimilation of rainfall forecasts were investigated by adopting the nested Local Ensemble Transform Kalman Filter (LETKF, Miyoshi and Aranami, 2006) to a local heavy rainfall that developed in the Osaka Plain, Japan, on 5th September 2008.

*a. Truth data and first guess data*

Figure 1a shows the horizontal distributions of 1-hour rainfall amount and wind distribution at the height of 20 m at 17 JST 5th September 2008 (Japan Standard Time, 9 JST corresponds to 0 UTC), at which the local heavy rainfall just occurred. This distribution is the analyzed fields of the nested LETKF (ensemble member #007) obtained by the assimilation of horizontal wind of Doppler radar and GPS-PWV data that were actually observed by "the Geospatial Information Authority of Japan" (GSI). Because the position and int ensity of the rainfall and northwestward extension of the rainfall region were similar to the observed ones, this distribution was used as the truth data. Figure 1b shows the horizontal distribution of results of LETKF obtained by assimilation of only the conventional data. Although the weak rainfall region extended to northwest, intense rainfall region extended in north-south direction developed in the northwestern part of the rainfall region. Because the intense rainfall region was not reproduced, this data was used as first guess fields.

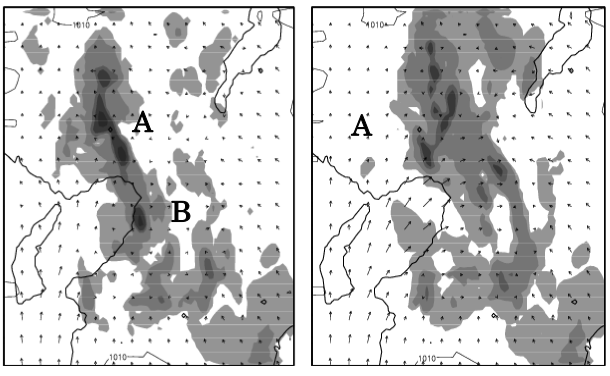


Fig. 1. Horizontal distributions of rainfall (shaded regions) and surface wind (vectors) of (a) truth data and (b) first guess data.

*b. Truth-derived SWV and PWV data*

From this truth data, GPS-derived SWV data (truth-derived GPS-SWV) and QZS-derived SWV (truth-derived QZS-SWV) were produced by integrating of water vapor along the path from GPS receivers to the satellites. The paths to the satellites were obtained on the assumption of the straight paths. In the estimation of truth-derived GPS-SWV data, the actually observed azimuth and elevation angles were used. As for truth-derived QZS-SWV, QZS position that is expected to be observed in Japan was used.

In the OSSE, not only the truth-derived SWV data, but also the truth-derived PWV was assimilated. The

truth-derived GPS-PWV data of each GPS receivers were obtained by converting the truth-derived GPS-SWV into the values of the zenith direction and by applying a gradient mapping function to them (Fig. 2a). The QZS-PWV data was estimated by the same method of the GPS-PWV data except that the QZS-SWV was added to the GPS-SWVs in the estimation of PWV (Fig. 2b).

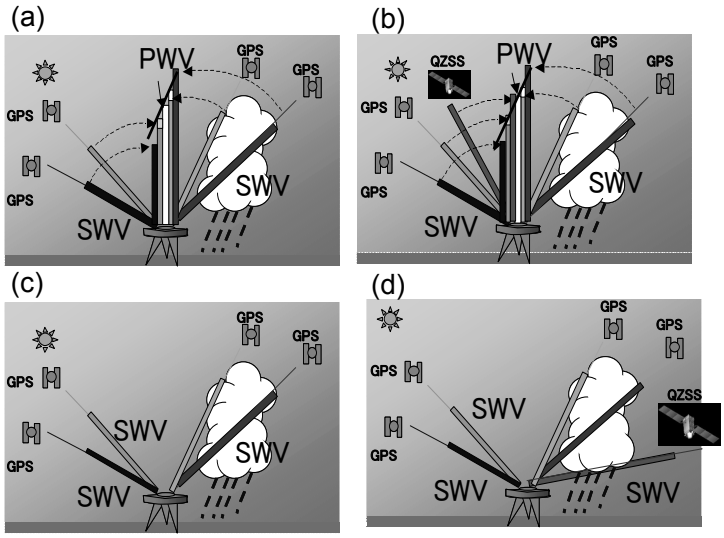


Fig. 2. Schematic illustrations of the assimilation data of (a) GPS-PWV and (b) QZS-PWV, and (c) GPS-SWV and (d) GPS-SWV and QZS-SWV.

## 3. Impacts QZS-derived PWV and SWV data on the local heavy rainfall

In the experiments on the PWV data, GPS-PWV and QZS-PWV were assimilated from 09 JST to 15 JST of 5th. As for QZS- SWV, the QZS data whose elevation angles were more than 60 degree were used. Figure 3 shows the analyzed rainfall regions obtained by assimilations of GPS-PWV or of QZS- PWV. When GPS-PWV or QZS-PWV was assimilated, the rainfall distribution became closer to the truth. Namely, the intense rainfall region (indicated by **A** in Fig. 3) had a branch extending southeastward, and the intense rainfall region south of **A** was also reproduced (indicated by **B** in Fig. 3). When QZS-PWV was assimilated, the intense rainfall **A** is more intensified and **B** became weaker, compared with those that were obtained by assimilation of GPS-PWV. These distributions obtained by the assimilation of QZS-PWV were more similar to the truth data. These results indicate that QZS- PWV data has the potential to improve the rainfall forecasts, though the impact was not larger because many GPS-derived data was already assimilated.

Impacts of the low-elevation data of QZS were shown in Fig. 4. Although the reproduced distribution was different from those of Fig. 3, the rainfall distributions became similar to the truth when GPS-derived or QZS-derived SWVs were assimilated. When QZS-derived data were added, the intense rainfall **A** is more intensified and **B** became weaker. Namely, the rainfall regions became more similar to the truth data. This result also indicates that QZS-derived SWV data also has the potential to improve the rainfall forecasts.

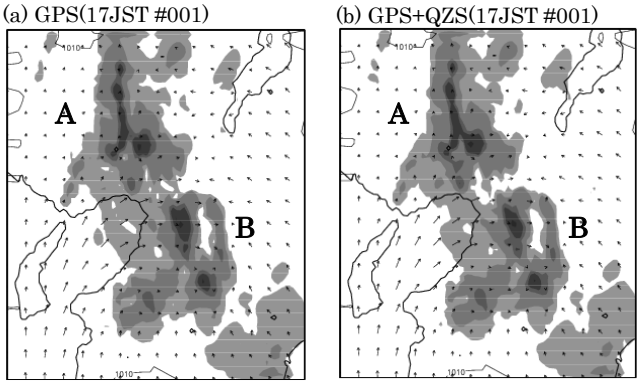


Fig. 3. Rainfall and horizontal wind distribution at 17 JST when (a) GPS-PWV and (b) QZS-PWV were assimilated.

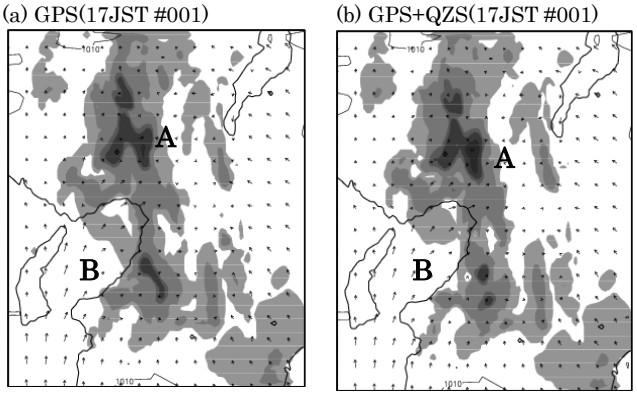


Fig. 4. Same as Fig. 3 except assimilations of (a) GPS-SWV and (b) QZS-SWV and GPS-SWV.


### Acknowledgements

The authors would like to express their gratitude to Mr. Kogure of JAXA, the Geospatial Information Authority of Japan and Osaka District Meteorological Observatory of JMA, which provided the QZS position data, GPS data and Doppler radar data. The improvements of severe weather forecasts (i.e. local heavy rainfalls), which were achieved by the assimilations of Doppler radars, will contribute to aviation safety and the mitigation of damages of other urban functions.


### Reference


Miyoshi, T. and K. Aranami, 2006: Applying a four-dimensional local ensemble transform Kalman filter (4D-LETKF) to the JMA nonhydrostatic model (NHM). SOLA, 2, 128-131.

# Impacts of the low-level convergence data on the local heavy rainfall

Hiromu Seko, Kazuo Saito, Osamu Suzuki and Ahoro Adachi (Meteorological Research Institute)

## 1. Introduction

One of the aims of the 'Social System Reformation Program for Adoption to Climate Change' project is to observe thunderstorms that cause local heavy rainfalls in urban areas (such as the Tokyo Metropolitan area) and to clarify the mechanisms of their generation, development and decay by using the observation data and outputs of numerical models. In the Nerima local heavy rainfall that occurred in 1998, the thunderstorms were generated by the convergence that was produced by a thermodynamic low. Because convergence started before the generation of the thunderstorms, it is expected that the thunderstorms can be reproduced before their generation when the large-scale convergence data was provided. In this study, the observation data of the airplane and of the low-level profilers in the urban area, which have the information of the horizontal convergence of the low-level wind, were assimilated and their impacts were investigated by checking that the generation and development of the thunderstorms were reproduced by the assimilation of these data.

## 2. Outline of the observation system simulation experiments

In the observation system simulation experiments of his study, three kinds of observation data were produced from the truth data (outputs of numerical model in which thunderstorm was well reproduced), and were assimilated into the first-guess (initial conditions in which the thunderstorm was not reproduced). The impact of observation data, namely how the thunderstorm is improved by the assimilation of the observation data was investigated.

In this study, the thunderstorm which was similar to the observed one was reproduced with the nested LETKF system by the assimilations of GPS precipitable water vapor data and of horizontal wind of Doppler radar. This data that was most similar to the observed one was used as the truth data. The following three observation data which surrounded the thunderstorm were produced from the truth data of 15 JST, 2 hour before the development of the thunderstorm. The first is the airplane data, which is water vapor, temperature, heading wind speed or horizontal wind at the height of 400 m at the circle points in Fig. 2a. Second one is the wind profiler data which is the horizontal winds below the height of 200 m at the same points of airplane data. And the last one is the thermo profiler data which is the temperature profiles below the height of 600 m at the same points of airplane data. These data was assimilated into the initial condition of 15 JST which were obtained by assimilation of the conventional data only.

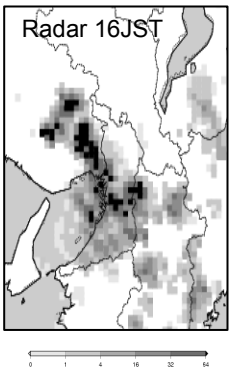


Fig. 1 Rainfall region of the thunderstorm at 16 JST 5th Sep. 2008 to which OSSE applied.

## 3. Impacts of low-level data which surrounded the generation point of the thunderstorm

When the airplane data or profiler data were assimilated, the thunderstorm was reproduced where it was observed. These results show that observation data surrounding the thunderstorm can improve their rainfall forecast even if the direct observation data of the thunderstorm was not used.

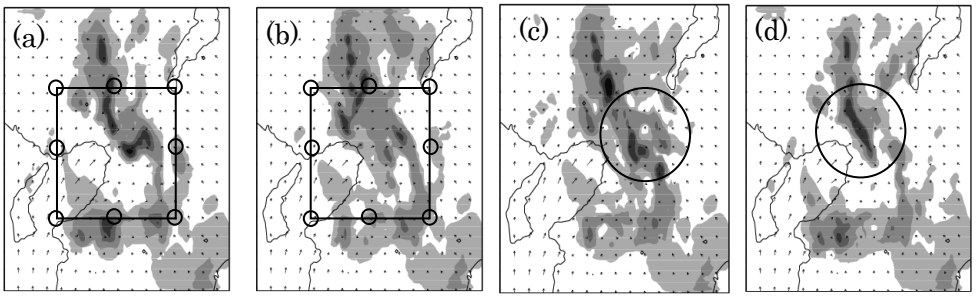


Fig 2: Results of OSSE. (a) Truth data obtained by the assimilation of the conventional data and GPS and Doppler radar data. (b) First guess data obtained by the assimilation of the conventional data. (c) and (d) Result of assimilations of truth-derived airplane data and truth-derived profiler data

**Acknowledgements**

The authors would like to express their gratitude to Mr. Kogure of JAXA, the Geospatial Information Authority of Japan and Osaka District Meteorological Observatory of JMA, which provided the QZS position data, GPS data and Doppler radar data. The improvements of severe weather forecasts (i.e. local heavy rainfalls), which were achieved by the assimilations of Doppler radars, will contribute to aviation safety and the mitigation of damages of other urban functions.

**Reference**

Miyoshi, T. and K. Aranami, 2006: Applying a four-dimensional local ensemble transform Kalman filter (4D-LETKF) to the JMA nonhydrostatic model (NHM). SOLA, 2, 128-131.

# Improvements of the nested LETKF system

- Impacts of GPS water vapor data and synergistic effects of GPS water vapor data and wind data -

Hiromu Seko, Tadashi Tsuyuki, Kazuo Saito (Meteorological Research Institute)

## 1. Introduction

The nested Local Ensemble Transform Kalman Filter system has been developed to improve the accuracy of numerical forecast on local heavy rainfalls. To reproduce local heavy rainfalls, their positions and rainfall intensities need to be improved, simultaneously. Mesoscale convergence, in which local heavy rainfalls are generated, was reproduced in this study by the Local Ensemble Transform Kalman Filter (LETKF) with the grid interval of 15 km (Outer LETKF). The convection cells that caused local heavy rainfall were reproduced by the LETKF with the grid interval of 1.875 km (Inner LETKF). The boundary conditions of the Inner LETKF were produced from the outputs of the Outer LETKF, and the results of the Inner LETKF influenced the Outer LETKF every 6 hours. To show the performance of this system, this system was applied to a thunderstorm that caused the local heavy rainfall on the Osaka Plain on 5th September 2008. Convergence of low-level water vapor is indispensable in reproducing local heavy rainfalls. GPS-derived PWV or SWV (slant path water vapor) and horizontal wind or radial wind observed by Doppler radars provide information about low-level convergence of water vapor. A number of data assimilation experiments on radial wind from Doppler radars and PWV using the EnKFs have been reported so far. In this study, the impacts of the SWV and the synergistic effect of simultaneous assimilation of Doppler radar data and GPS water vapor data (PWV or SWV) are investigated, as well as the GPS-PWV data and Doppler radar data.

## 2. Outlines of the nested LETKF system

This data assimilation system was composed of two NHM-LETKFs (Miyoshi and Aranami, 2006): the Outer and Inner LETKFs. The number of vertical layers was 50 and the depth of the vertical layers was increased from 40 m to 880 m as the height increased. The number of ensemble members was 12.

As for the Outer LETKF system, the grid interval is 15 km and the grid number in the horizontal directions was 80 × 80. The Kain-Fritch parameterization scheme was adopted. The ensemble forecast started at 0900 JST 1st September 2008 and the initial seed of the Outer LETKF was obtained from the JMA mesoscale analysis fields from 29th to 31st August. The boundary condition from 1st to 5th September was also produced from the JMA mesoscale analysis. The data assimilation window was 6 hours and the conventional data, which was used in the JMA mesoscale analysis, were assimilated every hour.

The grid interval of the Inner LETKF was as small as 1.875 km to resolve small convection cells. In the microphysical process, the mixing ratio of cloud, rain, ice crystals, graupel and the number density of ice crystals were predicted. The boundary conditions and first initial seed of the Inner LETKF were produced from the Outer LETKF. The data assimilation window is 1 hour, and three series of 6 cycles were performed from 03 JST 5th. In addition to the conventional data, GPS water vapor data and radar wind data were assimilated every 10 minutes.

To reflect the analysis of the Inner LETKF in the Outer LETKF, the analyzed value of the Outer LETKF was replaced by that of the Inner LETKF every 6 hours at the end of the assimilation windows of the Outer LETKF. To reduce the inconsistencies between the Inner and the Outer LETKFs, the values of the Outer LETKF near the boundary of the Inner LETKF were produced by blending with those of the Outer LETKF.

## 3. Impacts of GPS water vapor data and the synergistic effects of GPS water vapor data and wind data

*a. Impact of GPS water vapor data*

In this study, PWV and SWV estimated from the atmospheric delays (Shoji et al. 2004) were used as assimilation data. PWV and SWV are the integrated value of water vapor in the column or along the paths from GPS satellites to GPS receivers. Because LETKF cannot assimilate the non-local data (i.e. integrated value data, such as PWV) directly, water vapor at the points where the paths crossed each layer of LETKFs (intermediary data) was estimated, and then assimilated in the Inner LETKF. In the estimation of this input data, the following two assumptions were used; (1) Differences between input data and first guess are proportional to the spread of water vapor. Due to position errors of rainfall regions and large dispersion of water vapor distributions caused by small ensemble numbers, area-mean water vapor profile and area-maximum spread profiles of water vapor within the areas from 18 km from GPS receivers were used as the first guess and spread profiles of water vapor (Seko et al. 2011). (2) The input data is produced at the layers where the correlation among the ensemble members between water vapor of each layer and PWV exists (Fujita et al. 2011). The assimilation method of SWV was the same as that of PWV, except for the slant paths and the small areas that were used in producing the ensemble mean and maximum spread profiles of water vapor. Because SWV is water vapor between GPS satellites and receivers, SWV provides water vapor values as well as its direction. If large areas were used in producing the ensemble mean and maximum spread profiles, the direction would become ambiguous because large areas dilute this information. To exploit this advantage of SWV, areas used in producing ensemble mean and maximum spread were reduced from 18 km to 3 km.

Figure 1 is the analyzed rainfall distributions at 17 JST reproduced by the Inner LETKF to show the development of the rainfall on the Osaka Plain. In a few ensemble members, the intense rainfall regions on the Osaka Plain extended northwestward. This feature of the analyzed distributions, which was the same as the observed one at 16 JST, indicates that the local heavy rainfall on the Osaka Plain were well reproduced in a few members, though there

was a time lag of 1 hour.

Figure 2 shows the rainfall regions at 17 JST that were obtained by assimilation of PWV and SWV data. These data from 9 JST to 15 JST was assimilated in the Inner LETKF. When the PWV data was assimilated, the number of ensemble members in which the rainfall regions were extending northwestward increased. Especially, rainfall became more intense in most of ensemble members. When SWV data was assimilated, the number of ensemble forecasts in which the intense rainfalls were well reproduced was further increased in this study. It is deduced that some paths from GPS receivers to GPS satellites penetrated humid regions that generated the convection cells on the Osaka Plain.

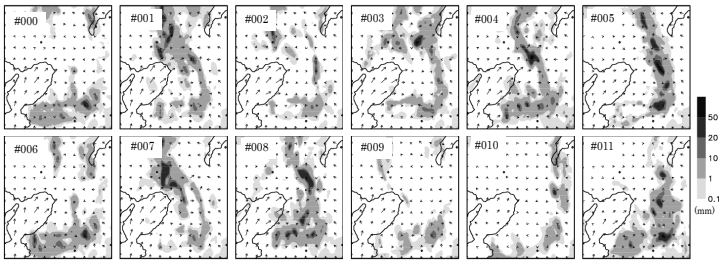


Fig. 1 Horizontal distributions of 1 hour rainfall and horizontal wind at the height of 20 m reproduced with the Inner LETKF by assimilation of conventional data.

*b. The synergistic effect of GPS water vapor data and Radial wind data*

As for the Doppler radar data, two kinds of data were assimilated. The first was the horizontal wind obtained by the dual analyses of the radial wind of Kansai and Osaka international airports. The second kind of data is radial wind of Doppler radar. This wind data is expected to be more effective to improve the rainfall forecasts because it provides the information from a wider area.

Figures 3a is the rainfall distributions at 17 JST that were obtained by the assimilation of the horizontal wind. The horizontal and radial winds were assimilated from 14 JST to 15 JST, because the rainfall regions were fewer and smaller before 14 JST. When the horizontal winds were assimilated, the number of ensemble members in which the intense rainfall regions extended northwestward was increased. When the radial winds were assimilated, the number was further increased though the rainfall intensity remained relatively weak (not shown). These results indicate that the wind data, especially radial wind, can improve rainfall forecasts.

Figure 3b is the rainfall distributions that were obtained by the simultaneous assimilation of the horizontal wind and PWV. When this data was assimilated, the rainfall forecasts in the ensemble members #007 and #011, in which the intense rainfall region was not reproduced by the individual assimilation of the PWV and horizontal wind, were improved. The improvements of rainfall forecasts in the ensemble members #002 and #003 became unclear, compared with those in which the PWV or horizontal wind was assimilated separately. However, the rainfall distributions of #002 and #003 remained better than those obtained from the assimilation of conventional data. These results indicate that the simultaneous assimilation is useful for increasing the number of members in which local heavy rainfalls are reproduced.

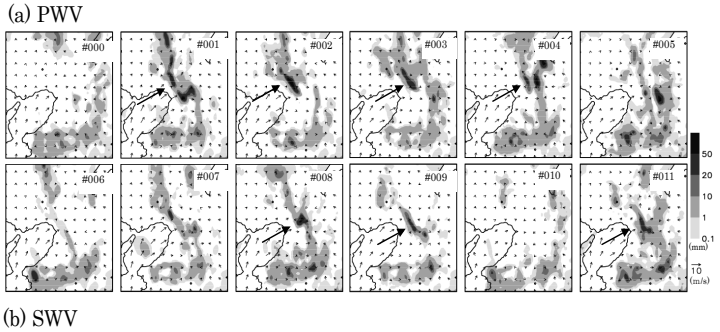


Fig. 2 Same as Fig. 1 except by adding (a) PWV data and (b) SWV data to the assimilation data.

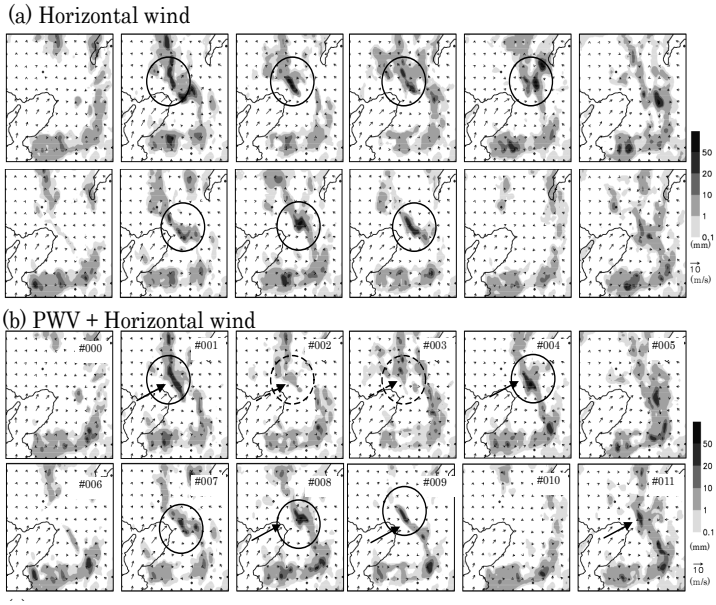


Fig. 3 Same as Fig. 1 except by adding of (a) horizontal wind and (b) horizontal wind and PWV data to the assimilation data.

**Acknowledgements:** The authors would like to express their gratitude to the Geospatial Information Authority of Japan and Osaka District Meteorological Observatory of JMA, which provided the GPS data and Doppler radar data. The improvements of severe weather forecasts, which were achieved by the assimilations of Doppler radar data, will contribute to aviation safety and the mitigation of damages of other urban functions.

**Reference**

Miyoshi, T. and K. Aranami, 2006: Applying a four-dimensional local ensemble transform Kalman filter (4D-LETKF) to the JMA nonhydrostatic model (NHM). SOLA, 2, 128-131.

# Data assimilation in a two-scale model with Kalman filters

Tadashi Tsuyuki
Meteorological Research Institute/JMA, E-mail: ttuyuki@mri-jma.go.jp

## 1. Introduction

Data assimilation in multi-scale models, such as a coupled ocean-atmosphere model and a global cloud-resolving atmospheric model, has a potential to improve large-scale analyses by assimilating small-scale observations through scale interactions. A problem is that multi-scale models are strongly nonlinear while most of the data assimilation methods used in geophysics assumes that probability density functions are nearly Gaussian.

Ballabrera-Poy et al. (2009) investigated the accuracy of analyses when both large- and small-scale variables are simultaneously assimilated with an ensemble Kalman filter by using a Lorenz-96 two-scale model (Lorenz, 1996). They found that assimilation of large-scale variables with a few small-scale variables significantly degraded the filter performance due to spurious correlations from sampled ensemble covariances.

The present study further investigated multi-scale data assimilation with Kalman filters. There is almost no difficulty in applying Kalman filters to numerical models which contain very different time scales, compared to 4-dimensional variational assimilation.

## 2. Method

Data assimilation experiments were conducted on a perfect model assumption with the Lorenz-96 two-scale model:

$$\frac{dX_k}{dt} = -X_{k-1}(X_{k-2} - X_{k+1}) - X_k + F - \frac{hc}{b}\sum_{j=1}^{J} Y_{jk} \qquad (k = 1, \cdots, K),$$

$$\frac{\mathrm{d}Y_{jk}}{\mathrm{dt}} = -cbY_{j+1\,k}\left(Y_{j+2\,k} - Y_{j-1\,k}\right) - cY_{jk} + \frac{hc}{b}X_k \qquad (j = 1, \cdots, J).$$

The parameter values used were $K = 36$, $J = 10$, $F = 10$, $h = 1$, $b = c = 10$ as in Lorenz (1996). The temporal and spatial scales and amplitude of $Y$ were about a tenth of those of $X$ in these parameters. The time integrations were conducted with a time step $\Delta t = 0.005$.

The assimilation methods used were a local ensemble transform Kalman filter (LETKF; Hunt et al., 2007) and an extended Kalman filter (EKF; Thornton and Bierman, 1980). EKF does not have sampling error, but has linearization error. The observational data of $X$ were available at a time interval of $10\Delta t$ at all coarse grid points with observation error standard deviation of unity. The impact of the temporal and spatial densities and error standard deviation of observations of $Y$ on the analyses of $X$ were examined. The assimilation period was $40{,}000\Delta t$.

## 3. Results

Figure 1 shows the average analysis errors of $X$ for the latter half period of assimilation experiments with LETKF with 10 ensemble members. The values of multiplicative inflation factor and the size of local patches were optimized so that the average analysis errors of $X$ were minimized under a constraint that the local patch size of $Y$ is a tenth of that of $X$. The figure demonstrates that if the spatial or temporal densities or accuracy of observational data of small-scale variables is not enough, a straightforward application of an ensemble Kalman filter ("with C.I.") tends to degrade the analysis of large-scale variables. In those cases better analyses are obtained by not assimilating the small-scale observations ("Obs of X only"). This result is consistent with that of Ballabrera-Poy et al. (2009), but it is not due to sampling error, because similar results were obtained from LETKF experiments with larger ensemble members such as 200 and 500. In those experiments, adaptive covariance inflation (Li et al., 2009) was used and local patches were not applied. Assimilation experiments with EKF with the adaptive covariance inflation also gave a qualitatively similar result. Those results suggest that the degradation of large-scale analysis is due to the Gaussian assumption of Kalman filters.

The figure also shows the results from assimilation experiments in which the cross analysis increments between large- and small-scale variables were neglected at the analysis step of LETKF ("w/o C.I."). Scale interactions in data assimilation were allowed only in the forecast step. If the

spatial and temporal densities and accuracy of observational data of small-scale variables were enough, the large-scale analyses were degraded compared to the previous experiments. If that was not the case, however, the neglect of cross analysis increments lead to better large-scale analyses than the analyses obtained from assimilating large-scale observational data only.

The neglect of cross analysis increments may be easily applied to a coupled ocean-atmosphere model, since most of the state variables are separated into oceanic and atmospheric variables. On the other hand, a hierarchical approach may be necessary for a global cloud-resolving atmospheric model, since it is not easy to extract cumulus-scale variables from the state variables. In the hierarchical approach, large-scale observational data are assimilated first to obtain large-scale analysis. Then small-scale observational data are assimilated with the large-scale analysis given, and the multi-scale model is integrated in the forecast step. It was found from LETKF experiments with the Lorenz-96 two-scale model that this approach gave analyses of similar quality to those obtained by neglecting the cross analysis increments.

## References


Ballabrera-Poy, J., E. Kalnay and S. C. Yang, 2009: Data assimilation in a system with two scales – Combining two initialization techniques, *Tellus*, **61A**, 539-549.

Hunt, B. R., E. J. Kostelich and I. Szunyogh, 2007: Efficient data assimilation for spatiotemporal chaos: A local ensemble transform Kalman filter, *Physica D*, **230**, 112-126.

Li, H., E. Kalnay and T. Miyoshi, 2009: Simultaneous estimation of covariance inflation and observation errors within an ensemble Kalman filter, *Q. J. R. Meteorol. Soc.*, **135**, 523-533.

Lorenz, E. D., 1996: Predictability – A problem partly solved, *Proceedings of the ECMWF Seminar on Predictability (4-9 September 1995, Reading, UK)*, ECMWF, 1-18.

Thornton, C. L. and G. J. Bierman, 1980: UDUT Covariance Factorization for Kalman Filtering, *Control and Dynamic Systems (C.T. Leondes, Ed.)*, **16**, 177-248.


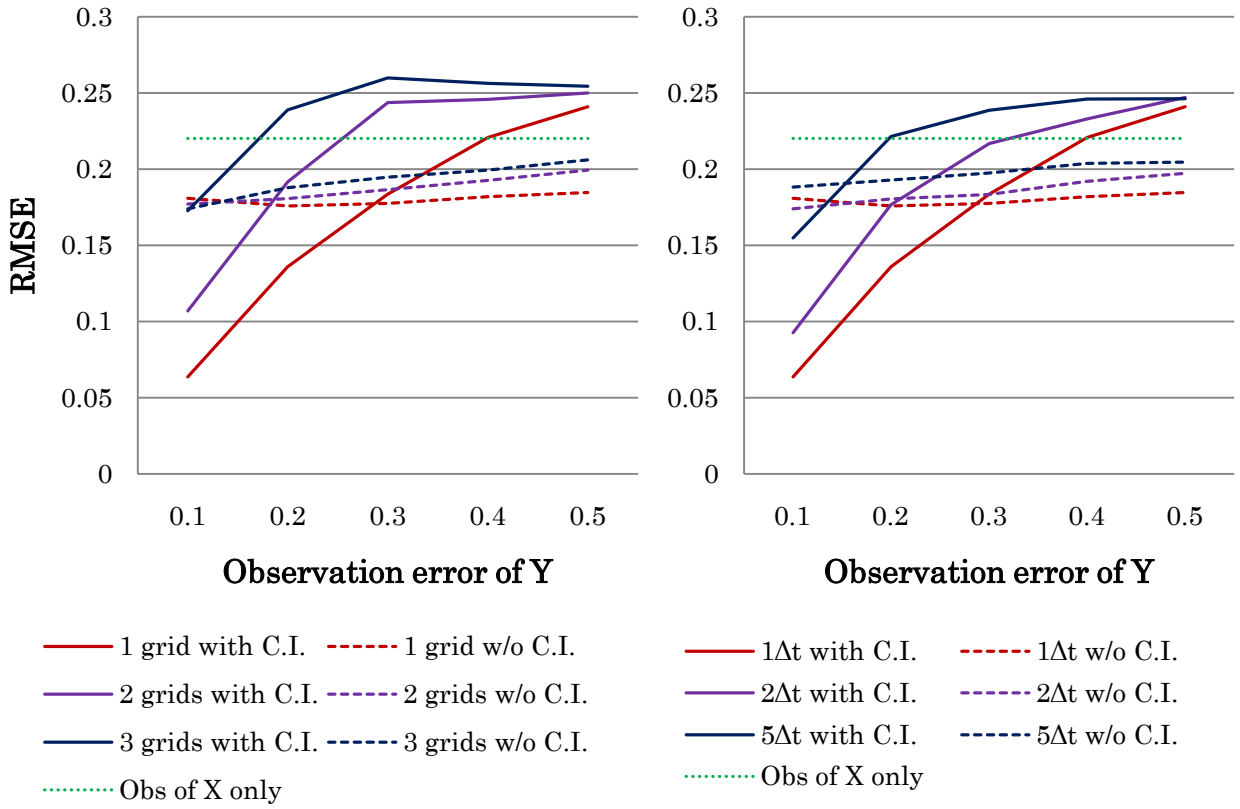


**Figure 1.** RMSE of analyses of $X$ averaged over 20,000 time steps and all grid points from assimilation experiments with LETKF with 10 ensemble members. The left panel shows the impact of grid interval and error standard deviation of observations of $Y$ when they are available at every time step. The right panel shows the impact of time interval and error standard deviation of observations of $Y$ when they are available at every grid point. "C.I." in the figure legends stands for the cross analysis increment between the variables of $X$ and $Y$.